EISCAT

EUROPEAN INCOHERENT SCATTER SCIENTIFIC ASSOCIATION

ANNUAL REPORT 2017 – 2018

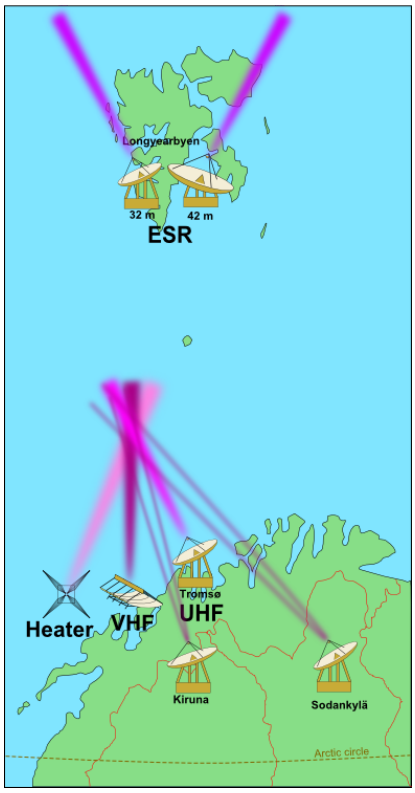

EISCAT Radar Systems

Location		Tromsø	Kiruna	Sodankylä	Longyearbyen	
Geographic coordinates		69°35′N 19°14′E	67°52′N 20°26′E	67°22′N 26°38′E	78°9′N 16°1′E	
Geomagnetic inclination		77°30′N	76°48′N	76°43′N	82°6′N	
Invariant latitude		66°12′N	64°27′N	63°34′N	75°18′N	
Band	UHF	VHF	VHF	VHF	UHF	
Frequency (MHz)	929	224	224	224	500	
Maximum bandwidth (MHz)	8	3	8	8	10	
Transmitter	2 klystrons	1 klystron	-	-	16 klystrons	
Channels	6	6	6	6	12	
Peak Power (MW)	2.0	1.6	-	-	1.0	
Average power (MW)	0.25	0.20	-	-	0.25	
Pulse duration (ms)	0.001–2.0	0.001–2.0	-	-	0.0005–2.0	
Phase coding	binary	binary	binary	binary	binary	
Minimum interpulse (ms)	1.0	1.0	-	-	0.1	
Digital processing	14 bit ADC on IF, 32 bit complex autocorrelation functions, parallel channels					
					Antenna 1	**Antenna 2**
Antenna	parabolic dish	parabolic cylinder	parabolic dish	parabolic dish	parabolic dish	parabolic dish
Feed system	32 m steerable Cassegrain	120 m × 40 m steerable line feed 128 crossed dipoles	32 m steerable crossed dipole	32 m steerable crossed dipole	32 m steerable Cassegrain	42 m fixed Cassegrain
System temperature (K)	90	250	100	100	80	65
Gain (dBi)	48.1	46	48.1	48.1	42.5	44.8
Polarisation	circular	circular	any	any	circular	circular

EISCAT Heating Facility (Tromsø)

Frequency range: 4.0 MHz to 8.0 MHz, Maximum transmitter power: 12×0.1 MW, Antennas: Array 1 (5.5 MHz to 8.0 MHz) 30 dBi, Array 2 (4.0 MHz to 5.5 MHz) 24 dBi, Array 3 (5.5 MHz to 8.0 MHz) 24 dBi.
Additionally, a Dynasonde is operated at the heating facility.

Cover picture: The opening event for the construction of EISCAT_3D took place on 7 September 2017 in Tromsø and Storfjord, Norway.

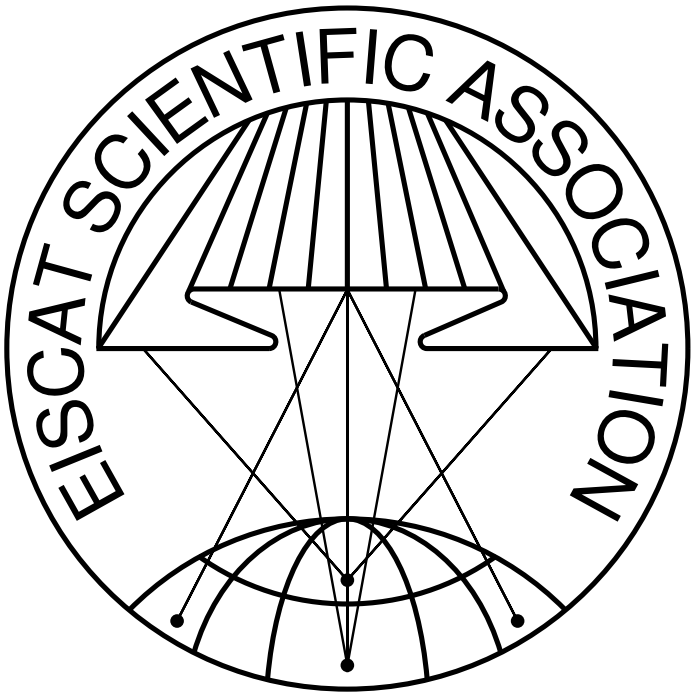

EISCAT Scientific Association
2017–2018

The high-latitude atmosphere and ionosphere represent both a critically important window on solar-terrestrial relationships and a vast natural plasma physics laboratory. The Arctic areas of northern Europe provide the easiest access to this available anywhere in the World, with well-developed infra-structure, extensive installed observational facilities, and a number of centres of academic excellence in appropriate fields.

The EISCAT Scientific Association was established in 1975 and its first incoherent scatter radar system became operational in 1981. Since then, the facilities of the EISCAT Scientific Association have been continuously developed and extended and today comprise world-class radars and a powerful ionospheric heating facility. Developments in hardware, software, and observational techniques have allowed the range of science addressed to be dramatically broadened since the first observations were made and the Association continues to provide and develop appropriate tools to support its user community. Access to the world-class EISCAT facilities is provided to all scientists in the Associate countries and to other Affiliates, and processed data products are made freely available to all. In this way, EISCAT has played a pivotal role in supporting research in many areas including solar-terrestrial relationships, solar system physics, geospace studies, space weather, and global change.

The scientific strategy of EISCAT is to understand the various forms of coupling between the Sun, the interplanetary medium, the terrestrial magnetosphere, ionosphere, and atmosphere of the high-latitude regions, natural and anthropogenic forcing, and related plasma physics and dynamics, and to achieve the necessary knowledge, understanding, principles, and techniques which would allow mankind to monitor, predict, and mitigate such processes within the next 30 years.

The specific goals of EISCAT are to develop large-scale facilities, techniques, and methods and, together with other ground-based and space-borne instruments, and as part of the global network of incoherent scatter and other middle and upper atmosphere radars, to encourage and undertake high quality research related to the global goal through studies addressing:

- *Behaviour and energy budget of the high-latitude regions, including space weather effects*
- *Fundamental plasma physics and dynamic processes in the near-Earth space environment*
- *Trends in atmospheric and ionospheric conditions, including long term/global change*
- *Properties and dynamics of the interplanetary environment*
- *Parametrisation of these processes and the development of techniques for their prediction*

The investments and operational costs of EISCAT are shared between:

China Research Institute of Radiowave Propagation, People's Republic of China
National Institute of Polar Research, Japan
Norges forskningsråd, Norway
Suomen Akatemia, Finland
UK Research and Innovation, United Kingdom
Vetenskapsrådet, Sweden

Contents

Director's pages **7**

Current events **9**
The EISCAT_3D opening event 9

Scientific highlights and list of publications 2017–2018 **11**
Dynamics of the ionosphere and the upper atmosphere 11
Energy, flux, and brightness of pulsating aurora measured at high time resolution 11
Identification of scintillation signatures on GPS signals originating from plasma structures detected with EISCAT incoherent scatter radar 11
Energetic electron precipitation and auroral morphology at the substorm recovery phase 12
On the contribution of thermal excitation to the total 630.0 nm emissions in the northern cusp ionosphere 13
Anomalous F region radar echoes and auroral precipitation 14
Simultaneous FPI and TMA measurements of the lower thermospheric wind in the vicinity of the poleward expanding aurora after substorm onset 14
PMSE dependence on frequency observed simultaneously with VHF and UHF radars in the presence of precipitation 15
Observations by incoherent scatter radar of related D- and F-region structuring at very high latitude 15
Electron energy spectrum and auroral power estimation from incoherent scatter radar measurements 16
GPS scintillations and losses of signal lock at high latitudes during the 2015 St. Patrick's Day storm 16
Tristatic observation of polar mesosphere winter echoes with the EISCAT VHF radar . . . 17
Depletion of mesospheric sodium during extended period of pulsating aurora 17
GPS scintillations associated with cusp dynamics and polar cap patches 18
. 18
Statistical study about the influence of particle precipitation on mesosphere summer echoes in polar latitudes during July 2013 19
Auroral molecular-emission effects on the atomic oxygen line at 777.4 nm 19
Seasonal and solar cycle variations of thermally excited 630.0 nm emissions in the polar ionosphere 20
Plasma line observations from the EISCAT Svalbard Radar during the International Polar Year 21
Polar cap patches observed by the EISCAT Svalbard Radar: A statistical study of its dependence on the solar wind and IMF conditions 21
Average field-aligned ion velocity over the EISCAT radars 22
Equatorward propagating auroral arcs driven by ULF wave activity: Multipoint ground- and space-based observations in the dusk sector auroral oval 22
Ionospheric response observed by EISCAT during the 6–8 September 2017 space weather event 23
Active experiments 24

The behavior of electron density and temperature during ionospheric heating near the fifth electron gyrofrequency . . . 24
Results of ionospheric heating experiments involving an enhancement in electron density in the high latitude ionosphere . . . 24
Survey of conditions for artificial aurora experiments at EISCAT Tromsø using dynasonde data . . . 25
The extending of observing altitudes of plasma and ion lines during ionospheric heating 25
Evidence of L-mode electromagnetic wave pumping of ionospheric plasma near geomagnetic zenith . . . 26
Systematic variation in observing altitude of enhanced ion line by the pump near fifth gyroharmonic . . . 26
First observations of recurring HF enhanced topside ion line spectra near the fourth gyroharmonic . . . 27
The polarization characteristics of ELF/VLF waves generated via HF heating experiments of the ionosphere by EISCAT . . . 27
Threshold of parametric instability in the ionospheric heating experiments . . . 28
Method developments . . . 28
Electron density inversed by plasma lines induced by suprathermal electron in the ionospheric modification experiment . . . 28
Background suppression and strong phase codes in incoherent scatter lag profile inversion 29
Publications 2017 . . . 30
Publications 2018 . . . 31

EISCAT Operations 2017 and 2018 **34**

EISCAT organisational diagram, 2016 **39**

Committee Membership and Senior Staff **41**

Appendix: EISCAT Scientific Association Annual Report, 2017 **43**

Appendix: EISCAT Scientific Association Annual Report, 2018 **59**

The EISCAT Associates and Affiliates, December 2018 **75**

Contact Information **76**

Director's pages

EISCAT continues to provide its user community with incoherent scatter radar (ISR) systems of the highest technical quality at key locations in the Geospace environment. The presently operating systems, in Ramfjordmoen (Norway), Kiruna (Sweden), Sodankylä (Finland) and Longyearbyen (Svalbard) have, of course, continued to be maintained and upgraded, but they are, to varying extents, showing their ages and have suffered from a number of repairable failures. This has resulted in some short-term data outages and performance limitations. For instance, several antenna issues have limited operations: the waveguide for the Ramfjordmoen VHF system had arcing problems, the pintle bearings in both the Ramfjordmoen UHF and the Sodankylä antennas have needed attention. Similarly, the antenna fields for the Heating facility have needed significant repairs to maintain operational status. Nonetheless, EISCAT has maintained successful measurement campaigns for Common Programmes, Special Programmes, and Per-review Programmes throughout this period.

Some time ago, EISCAT Council initiated an update to the EISCAT Blue Book, the document that lays out how the association is organized and operates. This new EISCAT Blue Book, Edition 2015, came into effect with the final signature on 20 June 2017. This version can be accessed via the EISCAT website, `www.eiscat.se`, and it includes a number of changes to the rules governing the association, including changes to several of the standing and temporary committees. Some of the changes are aimed at preparing for a new EISCAT_3D system which will replace the mainland sites.

The European Commission-funded EISCAT_3D Preparation for Production (EISCAT3D_PfP) project came to completion in August 2017 with numerous valuable lessons learned. While the final test subarray itself did not entirely fulfil the system design goals, the process of producing it illuminated a number of deficiencies in the specifications for the subsystems and also pointed toward the need to allocate sufficient time for thorough testing of those subsystems both before and after integration. The project itself also suffered from a number of delays, both in personnel hiring and in production, that worked against the hard deadline of the end date for the funding. During its execution, however, the project developed a tendering process that was fair, rapid, straightforward, and expandable to the full system implementation. It also uncovered some severe deficiencies in the earlier antenna design when that antenna was subjected to high power RF signals. These deficiencies must be addressed before the system implementation can move forward.

Efforts toward funding the EISCAT_3D implementation were finally successful and EISCAT Council instructed HQ to proceed with implementation in a resolution signed on 1 June 2017. The start of implementation was set to 1 September 2017 and a kickoff, hosted by The Arctic University of Norway (UiT), was held in Tromsø and Skibotn on 7 September. After many years of effort by a host of dedicated individuals, this finally initiates the building of this innovative new infrastructure.

The final quarter of 2017 saw the EISCAT_3D project move forward in earnest. Interviews were held for the key position of Project Leader and that role was filled by Mr. Johan Svensson starting 15 January 2018. EISCAT moved several EISCAT3D_PfP staff over to the implementation project and hired an additional staff member to take the lead on the software side of the project.

All but one of the major contracts for the EISCAT_3D Subarray subsystems were signed during 2018. Due to staffing bottlenecks, the tenders were handled serially, with the first tendering opportunity opened for the longest lead-time subsystem, the second for the second longest, and so on. The Antenna Unit (AU) contract was signed in March 2018, the First Stage Receive Unit (FSRU) was signed in June 2018, and the Subarray Transmit Unit (SAT) contract was signed in November 2018.

EISCAT is also receiving support for EISCAT_3D via a project with the Nordic e-Infrastructure Collaboration (NeIC). This project

is providing advice about high-bandwidth connectivity to the three initial sites as well as with possible architectures for data processing and data archiving.

Finally, EISCAT_3D took the significant step of becoming an ESFRI Landmark project in 2018. This demonstrates the importance of this new research infrastructure to the European research landscape and shows ESFRI's confidence in the scientific progress it promises.

Craig Heinselman
Director
EISCAT Scientific Association

Current events

The EISCAT_3D opening event

The opening event for the construction of the first stage of the EISCAT_3D system was held in Tromsø and Storfjord, Norway, on 7 September 2017.

The day started in brilliant sunshine with a bus transport to UiT, the Arctic University of Norway, where the first part of the opening event was held. Anne Husebekk, the university rector, greeted us all welcome and Ingrid Mann, the leader of the Norwegian project consortium, presented a general overview of the EISCAT_3D project. This was followed by short addresses from representatives of the EISCAT associate countries where it was clear that there are high expectations from the EISCAT user community of the future use of the new system. Finally, Craig Heinselman, EISCAT director, detailed the implementation of the EISCAT_3D system. Coffee and a selection of carrot and chocolate cakes were available at the mid-session break.

The opening event continued with a 90 minute long coach ride to the UiT Skibotn field station with a guide pointing out several interesting geological details in the local and regional geography. The sunshine was still accompanying us.

At the field station, the official opening ceremony for the project was held. This included speeches by Knut Jentoft, the mayor of Storfjord municipality, and Craig Heinselman, and the unveiling of an EISCAT_3D plaque. This part of the programme also contained musical performance with birch-bark horn and yoiking. After some refreshments, sparkling drinks and sandwiches, we were first guided to the location where the core array will be built and then transported to Storfjord shooting club in Hatteng for lunch. The food was a plate filled with local delicacies and we received more addresses from the university, the municipality, and EISCAT. There were also more musical entertainment covering the three different cultural traditions in the local area: the Norwegian, the Sami, and the Kven.

An EISCAT_3D plaque was unveiled at the UiT Skibotn field station.

On the journey back to Tromsø, we stopped at the EISCAT site at Ramfjordmoen to see the EISCAT_3D test array that was recently installed there. This was also a golden opportunity for a group photo thanks to the ever-present sun and the general good mood of the event participants.

The final part of the opening event day was a dinner at restaurant Scandic Ishavshotell. Several dinner courses and dinner speeches later, the evening was concluded with a nice auroral display as if the ionosphere itself wanted to celebrate the beginning of the EISCAT_3D construction project. This was certainly a fitting final of a good starting day for an exciting project.

Group photo of EISCAT_3D kick-off participants in front of the EISCAT_3D test array at the EISCAT site in Ramfjordmoen on 7 September 2017.

Scientific highlights and list of publications 2017–2018

Dynamics of the ionosphere and the upper atmosphere

Energy, flux, and brightness of pulsating aurora measured at high time resolution

Dahlgren et al. used high-resolution multispectral optical and incoherent scatter radar data to study the variability of pulsating aurora (Figure 1). They studied two events and combined the data with electron transport and ion chemistry modelling to provide estimates of the energy and energy flux during the bright and dark periods of the pulsations (the ON and OFF periods). Fits of the models to profiles of the ionization rate estimated from EISCAT UHF data are shown in Figure 2. Both the energy and energy flux were found to be reduced during each OFF period compared with the ON period, and the estimates indicate that it is the number flux of foremost higher-energy electrons that is reduced. The energies were found never to drop below a few kilo-electronvolts during the OFF periods for these events. The high-resolution optical data show the occurrence of dips in brightness below the diffuse background level immediately after the ON period has ended. Each dip lasts for about a second, with a reduction in brightness of up to 70 % before the intensity increases to a steady background level again. A different kind of variation is also detected in the OFF period emissions during the second event, where a slower decrease in the background diffuse emission is seen with its brightness minimum just before the ON period, for a series of pulsations. Since the dips in the emission level during OFF are dependent on the switching between ON and OFF, this could indicate a common mechanism for the precipitation during the ON and OFF phases. A statistical analysis of brightness rise, fall, and ON times for the pulsations is also performed. It is found that the pulsations are often asymmetric, with either a slower increase of brightness or a slower fall.

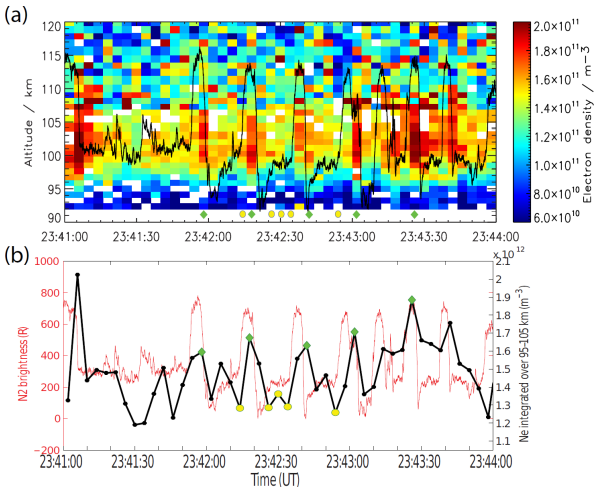

Figure 1: (a) electron density as a function of time and altitude, as measured by EISCAT on 22 October 2006. IN2 from ASK is overplotted in black. (b) Temporal evolution of electron density integrated over 95 km to 105 km (black) and ASK IN2 (red). Green diamonds mark the data dumps averaged to investigate the electron profile during bright periods whilst the yellow circles mark the selected data points for dark periods.

Dahlgren, H., B. S. Lanchester, N. Ivchenko, and D. K. Whiter, "Variations in energy, flux, and brightness of pulsating aurora measured at high time resolution", Ann. Geophys., 35, 493–503, doi:10.5194/angeo-35-493-2017, 2017.

Identification of scintillation signatures on GPS signals originating from plasma structures detected with EISCAT incoherent scatter radar

Ionospheric scintillation originates from the scattering of electromagnetic waves through spatial gradients in the plasma density distribution, drifting across a given propagation direction. Ionospheric scintillation represents a disruptive mani-

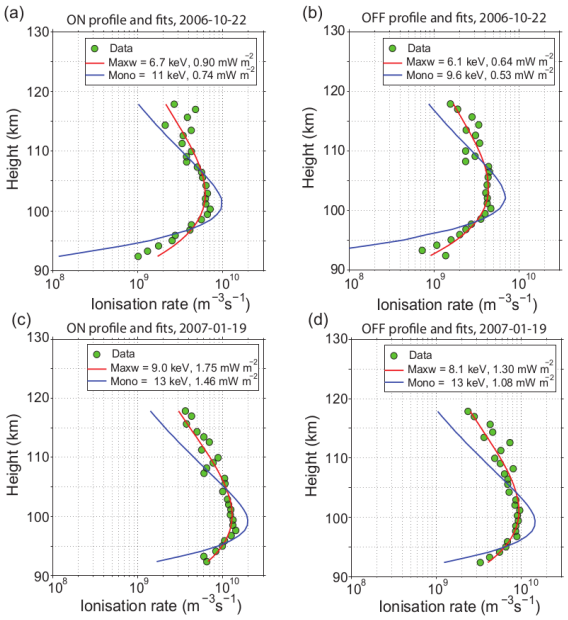

Figure 2: (a) Ionisation rate profile from EISCAT electron density data averaged over five measurements during ON periods is shown as green dots from the 2006 event. The line plots are the best fits to the data, as derived with a Maxwellian (red plot) and monoenergetic (blue plot) distribution of the electron spectrum. (b) Same as in (a), but for five averaged electron density profiles during OFF periods of the pulsations. (c) Same as in (a), but for the 2007 event. (d) Same as in (b), but for the 2007 event.

festation of adverse space weather conditions through degradation of the reliability and continuity of satellite telecommunication and navigation systems and services (e.g., European Geostationary Navigation Overlay Service, EGNOS). Forte et al. used EISCAT in conjunction with a GPS link to determine the contribution of auroral ionization structures to GPS scintillation (Figure 3). EISCAT measurements were made along the same line of sight of a GPS satellite observed from Tromsø and followed by means of the EISCAT UHF radar to causally identify plasma structures that give rise to scintillation on the co-aligned GPS radio link (Figure 4). Large-scale structures associated with the poleward edge of the ionospheric trough, with auroral arcs in the nightside auroral oval and with particle precipitation at the onset of a substorm were indeed identified as responsible for enhanced phase scintillation at L band. For the first time it was observed that the observed large-scale structures did not cascade into smaller-scale structures, leading to enhanced phase scintillation

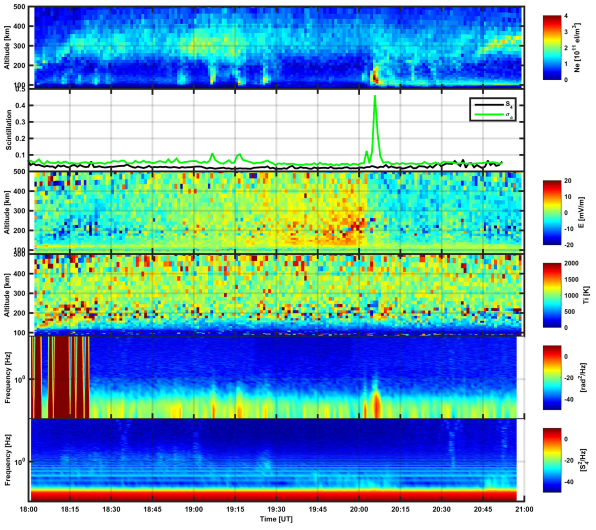

Figure 3: An event measured on 17 October 2013. From top to bottom: electron density profiles, GPS scintillation indices, electric field, ion temperature, PSD for the detrended carrier phase, and PSD for the normalized intensity. Some of the electron density structures had a corresponding scintillation signature, particularly the more intense features.

without amplitude scintillation. More measurements and theory are necessary to understand the mechanism responsible for the inhibition of large-scale to small-scale energy cascade and to reproduce the observations. This aspect is fundamental to model the scattering of radio waves propagating through these ionization structures. New insights from this experiment allow a better characterization of the impact that space weather can have on satellite telecommunications and navigation services.

Forte, B., C. Coleman, S. Skone, I. Häggström, C. Mitchell, F. Da Dalt, T. Panicciari, J. Kinrade, and G. Bust, "Identification of scintillation signatures on GPS signals originating from plasma structures detected with EISCAT incoherent scatter radar along the same line of sight", J. Geophys. Res. Space Physics, 122, 916–931, doi:10.1002/2016JA023271, 2017.

Energetic electron precipitation and auroral morphology at the substorm recovery phase

It is well known that auroral patterns at the substorm recovery phase are characterized by diffuse or patch structures with intensity pulsation. According to satellite measurements and simu-

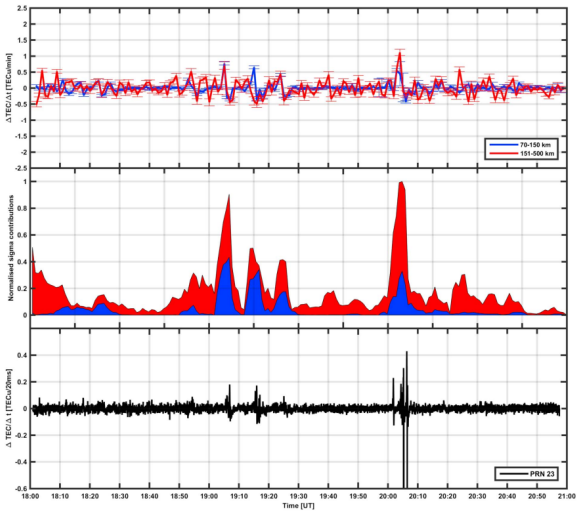

Figure 4: An event measured on 17 October 2013. (top) Temporal fluctuations in the radar TEC obtained integrating EISCAT electron density profiles for the E region (blue line) and the F region (red line), with error bars. (middle) The phase fluctuations originated from the E region (blue area) and the F region (red area). (bottom) The 50 Hz TEC temporal fluctuations on PRN32.

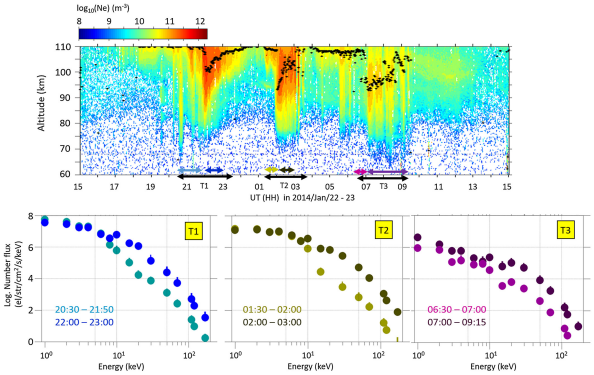

Figure 5: (top) Electron density measured with the EISCAT VHF radar at 60 km to 110 km height for 24 h from 15 UT on 22 January 2014. Black dots present a height where the electron density peaks during each integration period (1 min). The three selected time intervals, T1–T3 are separated into six groups as marked by colored arrows. (bottom row) Mean energy fluxes calculated with the CARD method using the electron density at individual six time intervals. The six time intervals are written in each panel.

lation studies, the precipitating electrons associated with these aurorae can reach or exceed energies of a few hundreds of keV through resonant wave-particle interactions in the magnetosphere. However, because of difficulty of simultaneous measurements, the dependency of energetic electron precipitation (EEP) on auroral morphological changes in the mesoscale has not been investigated to date. In order to study this dependency, we have analyzed data from the European Incoherent Scatter (EISCAT) radar, the Kilpisjärvi Atmospheric Imaging Receiver Array (KAIRA) riometer, collocated cameras, ground-based magnetometers, the Van Allen Probe satellites, Polar Operational Environmental Satellites (POES), and the Antarctic-Arctic Radiation-belt (Dynamic) Deposition-VLF Atmospheric Research Konsortium (AARDDVARK). Here we undertake a detailed examination of two case studies. The selected two events suggest that the highest energy of EEP on those days occurred with auroral patch formation from postmidnight to dawn, coinciding with the substorm onset at local midnight. Measurements of the EISCAT radar showed ionization as low as 65 km altitude, corresponding to EEP with energies of about 500 keV. See Figure 5.

S.-I. Oyama, A. Kero, C. J. Rodger, M. A. Clilverd, Y. Miyoshi, N. Partamies, E. Turunen, T. Raita, P. T. Verronen, and S. Saito, "Energetic electron precipitation and auroral morphology at the substorm recovery phase", Journal of Geophysical Research: Space Physics 122, 6508–6527, doi:10.1002/2016JA023484, 2017.

On the contribution of thermal excitation to the total 630.0 nm emissions in the northern cusp ionosphere

Kwagala et al. used simultaneous observations of the cusp using the EISCAT Svalbard radar (ESR) and meridian Scanning Photometer (MSP) located at the Kjell Henriksen Observatory (KHO) to calculate the contributions to the 630.0 nm auroral emission from thermally excited atomic Oxygen $O(^1D)$. They presented two case studies and derived the thermal contribution to the 630.0 nm emission using ESR electron temperature and density measurements. This was then compared to the 630.0 nm intensity from the MSP data (which contains both the thermal and collisional contributions). For both events the calculated thermal component had a correlation coefficient greater than 0.8 to the total observed 630.0 nm intensity. Despite fairly constant solar wind, the calculated thermal component intensity fluctuated possibly due to dayside transients in the aurora. Figure 10 shows the calculated volume emission rate as a function of altitude (panel a) and the cal-

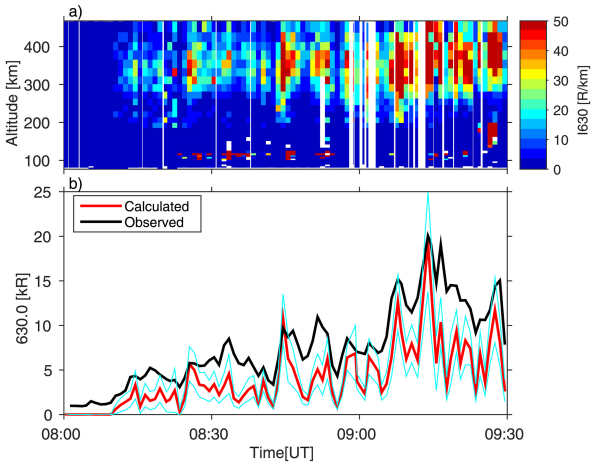

Figure 6: (a) The calculated volume emission rate versus height and (b) a comparison of the calculated thermal component with the MSP observations for event 1 on 22 January 2012. The cyan lines mark the upper and lower limits of the error bars of the calculated thermal component.

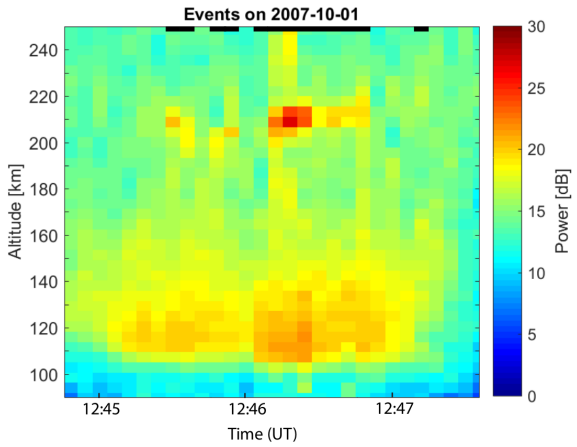

Figure 7: Received backscattered power as a function of time and altitude on 1 October 2007. In addition to the E region ionization, strong backscatter enhancements are found in a thin layer at around 210 km altitude. The data dumps with detected anomalous echoes are marked with black bars at the top of the plot.

culated thermal component in comparison to the observed (MSP) observations.

Kwagala, N. K., K. Oksavik, D. A. Lorentzen, and M. G. Johnsen, "On the contribution of thermal excitation to the total 630.0 nm emissions in the northern cusp ionosphere", J. Geophys. Res. Space Physics, 122, 1234–1245, doi:10.1002/2016JA023366, 2017.

Anomalous F region radar echoes and auroral precipitation

Non-thermal echoes in incoherent scatter radar observations are occasionally seen in the high-latitude ionosphere. Such anomalous echoes are a manifestation of plasma instabilities on spatial scales matching the radar wavelength. An example of spatially localized anomalous echoes with an enhanced zero Doppler frequency feature is shown in Figure 7. The occurrence of this class of anomalous echoes and the relation with auroral particle precipitation were investigated. The ionization profile of the E region is used to parametrize the precipitation, with nmE and hmE being the E region peak electron density and the altitude of the peak, respectively. The occurrence rate of the echoes generally increased with nmE and decreased with hmE, thereby indicating a correlation between the echoes and high-energy flux precipitation of particles with a high characteristic energy. The highest occurrence rate of larger than 20 % is found for $\mathrm{hmE} = 109\,\mathrm{km}$ and $\mathrm{nmE} = 10^{11.9}\,\mathrm{m}^{-3}$, averaged over the radar observation volume.

Dahlgren, H., N. M. Schlatter, N. Ivchenko, L. Roth, and A. Karlsson, "Relation of anomalous F region radar echoes in the high-latitude ionosphere to auroral precipitation", Ann. Geophys., 35, 475–479, doi:10.5194/angeo-35-475-2017, 2017.

Simultaneous FPI and TMA measurements of the lower thermospheric wind in the vicinity of the poleward expanding aurora after substorm onset

Lower thermospheric wind fluctuations in the vicinity of an auroral arc immediately before and after a substorm onset were examined by analyzing data from a ground-based green line Fabry-Perot interferometer (FPI; optical wavelength of 557.7 nm) at Tromsø, Norway, and in situ measurements from a trimethyl aluminum (TMA) trail released from a sounding rocket launched during the Dynamics and Energetics of the Lower Thermosphere in Aurora 2 (DELTA-2) campaign on 26 January 2009 (Figure 8). Soon after the rocket launch but before disappearance of the TMA trail, a substorm onset occurred. The DELTA-2 TMA experiment appears to be the first case in which the substorm onset occurred during the TMA wind measurement. It is known that energy dissipation induced by the ionospheric closure current is com-

pacted at the poleward side of the discrete arc in the ionospheric morning cell. Both FPI and TMA measurements were made at the poleward side, but the FPI measured winds nearer to the poleward edge of the arc than the TMA by 110 km to 130 km. The FPI winds at distance of 53 km to 74 km relative to the arc edge showed clear fluctuations immediately after the substorm onset, but there was no obvious similar fluctuation in the TMA-measured winds. The difference in the response at the two locations suggests that energy dissipation sufficient to be detected as the FPI/TMA wind perturbations was confined to the area from the poleward edge of the arc to a relative distance shorter than 163 km to 203 km but longer than 53 km to 74 km in this event.

Oyama, S., Kubota, K., Morinaga, T., Tsuda, T. T., Kurihara, J., Larsen, M. F., M. Yamamoto, and L. Cai, "Simultaneous FPI and TMA Measurements of the Lower Thermospheric Wind in the Vicinity of the Poleward Expanding Aurora After Substorm Onset", J. Geophysical Res., doi:10.1002/2017JA024613, 2017.

PMSE dependence on frequency observed simultaneously with VHF and UHF radars in the presence of precipitation

Using PMSE observations in combination with particle flux measurements obtained with detectors onboard GOES, a special condition is shown for the occurrence of the rarely observed UHF PMSE. When electron flux observed from GOES show a decrease after being in the presence of precipitation, UHF PMSE occurs. The heating effect on PMSE is small when the UHF electron density is enhanced at 90 km due to particle precipitation. We analyzed and compared the frequency dependence of PMSE under the condition of high energy particle precipitation in July of 2004 and 2007 at well separated frequencies (224 MHz and 930 MHz) at the same site, height, and time. The frequency index varies with height and time. At different heights, the maximum as well as the minimum value of volume reflectivity at VHF is greater than that at UHF with 2 to 3 orders of magnitude. A new qualitative method for the analysis of dust distribution is used by analyzing the relationship between volume reflectivity and frequency index. In agreement with the results of the model it is shown that dust particles of smaller size generally did not occur at the edges, instead they occurred in the middle PMSE regions.

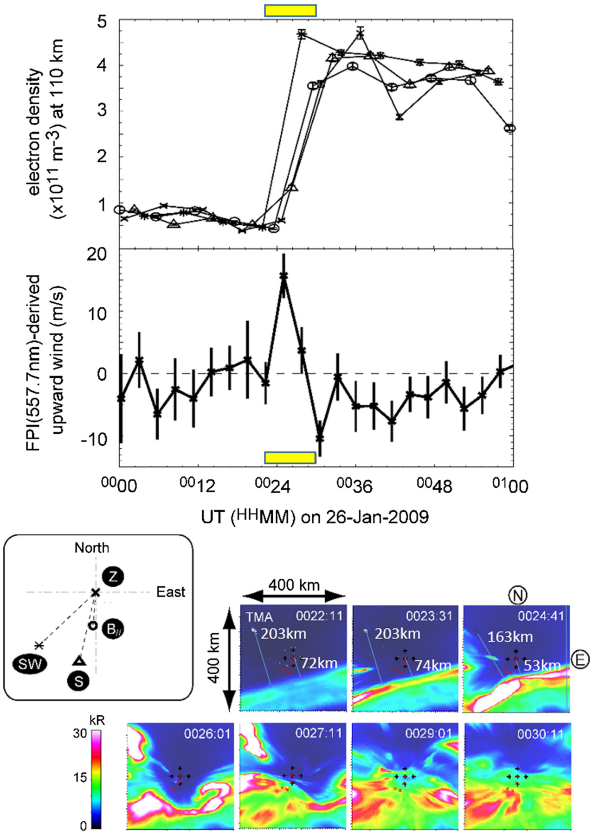

Figure 8: (first and second panels) The EISCAT-measured electron density measured at 110 km height and the FPI-measured upward wind speed (557.7 nm) from 00 UT to 01 UT on 26 January 2009. The EISCAT radar was sequentially directed at four positions as presented in the interpolated graph. (third and fourth panels) The horizontal pattern of the emission intensity measured with an all-sky camera (557.7 nm) from 00:22 UT to 00:30 UT. The time interval of the auroral images is marked in the first and second panels with horizontal yellow thick bars. Red and black crosses in the third and fourth panels are marked at positions measured with the EISCAT radar and the FPI, respectively.

Safi Ullah, Hailong Li, Abdur Rauf, Lin Meng, Bin Wang and Maoyan Wang, "PMSE dependence on frequency observed simultaneously with VHF and UHF radars in the presence of precipitation", Plasma Sci. Technol., 20, 115302, doi:10.1088/2058-6272/aac8d4, 2018.

Observations by incoherent scatter radar of related D- and F-region structuring at very high latitude

Hargreaves and Birch used the EISCAT Svalbard Radar to study a period of weak electron precip-

itation that led to an absorption layer between 80 km and 85 km. They inverted the electron density profile from the ESR to estimate the energetic electron spectrum responsible for the precipitation and concluded that the source was the solar wind. Variations in the D-layer electron density were accompanied by similar variations in the F-layer; this suggested that the electron flux reaching the D-region is being modulated in energy by the variations of electron density in the F-region.

Hargreaves, J. K., M. J. Birch, "Observations by incoherent scatter radar of related D- and F-region structuring at very high latitude", J. Atmos. Sol.-Terr. Phys., 174, 5–16, doi:10.1016/j.jastp.2018.01.032, 2018.

Electron energy spectrum and auroral power estimation from incoherent scatter radar measurements

We have developed a software package called ELSPEC for estimating differential energy spectra of precipitating electrons from EISCAT incoherent scatter radar data. The technique is based on analytic integration of the electron continuity equation and automatic spectrum model selection by means of the Akaike information criterion. The model does not assume balance between electron production and loss, and is thus well suited for observations of rapid changes in the auroral precipitation. In two case studies, the ELSPEC results were found to match well with electron energy spectra observed with the Reimei satellite and the with upward FAC observed with SWARM (Figure 9).

Ilkka I. Virtanen, Björn Gustavsson, Anita Aikio, Antti Kero, Kazushi Asamura, and Yasunobu Ogawa, "Electron energy spectrum and auroral power estimation from incoherent scatter radar measurements", J. Geophys. Res. Space Physics, 123, doi:10.1029/2018JA025636, 2018.

GPS scintillations and losses of signal lock at high latitudes during the 2015 St. Patrick's Day storm

Jin et al. investigated Global Positioning System (GPS) amplitude and phase scintillations during a severe geomagnetic storm on 17 March 2015. They related the total electron content (TEC) fluctuations, amplitude, and phase scintillation as measured by the GPS system to specific ionospheric density enhancements observed using the EISCAT Tromsø UHF radar. The strongest amplitude and

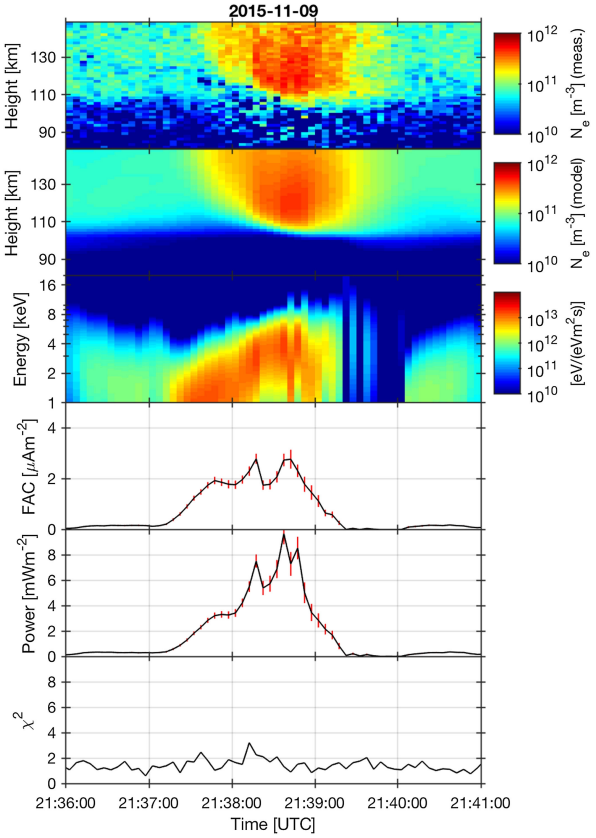

Figure 9: Inversion results during the Swarm C overflight on 9 November 2015. Electron density observed with EISCAT (top panel), electron density modeled in the inversion (second panel), differential energy flux (third panel), upward FAC (fourth panel), total energy flux (fifth panel), and χ^2 (bottom panel). The red vertical bars in the fourth and fifth panel are 1-σ error estimates. The satellite crossed the EISCAT geomagnetic latitude at 21:38:39 UT.

phase scintillations were observed when a TEC blob propagated across the field of view, whilst specific strong amplitude and phase scintillations were observed near the edges of the TEC blob. EISCAT observed significant enhancements in the F_2 region electron density near the edge of the TEC blob, while the E region was only slightly enhanced. This indicates that the plasma processes and instability modes, which accounted for the strong GPS scintillations, should involve the F_2 region ionosphere. Figure 10 shows data from the EISCAT radar during the two events used in the study (marked as time periods I and II in the figure).

Jin, Y., K. Oksavik, "GPS scintillations and losses of signal lock at high latitudes during the 2015 St. Patrick's

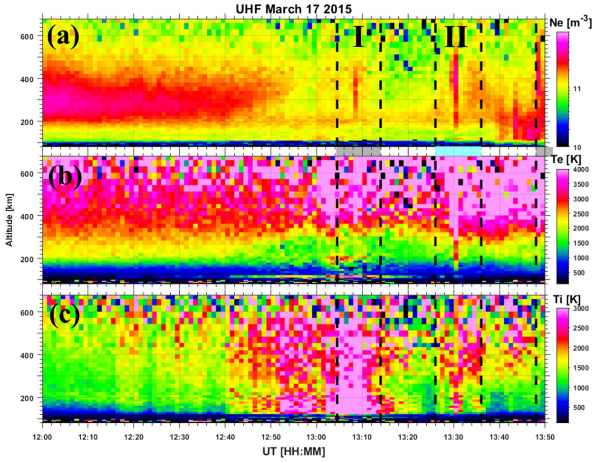

Figure 10: The EISCAT UHF data: (a) electron density (N_e), (b) electron temperature (T_e), and (c) ion temperature (T_i). The radar was pointing in a fixed direction (azimuth 185°, elevation 77°), which corresponds to the magnetic field aligned direction in the F region.

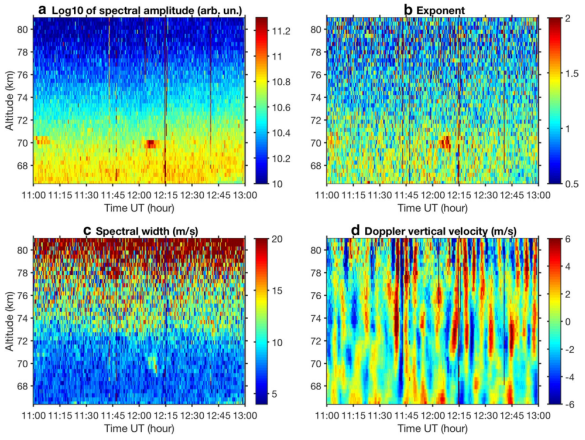

Figure 11: Time–altitude plot of fitted spectral amplitude (a), exponent (b), full spectral width (c) and vertical velocity (d) for Tromsø. The (almost) vertical lines at 11:44, 11:46, 12:02, 12:14 and 12:40 UT indicate range aliased echoes of space debris.

Day storm", Journal of geophysical research: Space physics, 123(9), 7943–7957, doi:10.1029/2018JA025933, 2018.

Tristatic observation of polar mesosphere winter echoes with the EISCAT VHF radar

Polar mesosphere winter echoes (PMWE) were observed at 70 km over Tromsø, Norway, on 8 January 2014 using the tristatic configuration of the European incoherent scatter VHF radar. For the interval 11:00 UT–13:00 UT where the strongest patch of PMWE of about 6 min duration was detected, the spectra of the received signal were analysed for the Tromsø site and altitude profiles of spectral parameters were derived, shown in Figure 11. For the remote sites Kiruna and Sodankylä, the Doppler velocities and their vertical shear were determined by using the measured autocorrelation functions. Ducted gravity waves with periods of 5 min to 10 min were found in the vertical wind velocity from 66 km to 81 km altitudes. The duct might be formed around 70 km and 77 km altitude where horizontal wind maxima were observed with the Kiruna receiver. However, no close relation between wind shear at 70 km altitude and PMWE at the same height was found: the wind shear was present for 2 h, but PMWE for only 6 min. Enhanced spectral width in the vertical Tromsø beam was observed for the PMWE patch. These experimental findings were discussed in relation to the winter echo generation mechanism. The conclusion was that the presence of patchy negatively charged small-sized dust might explain the observations although a gravity wave breaking mechanism cannot be completely rejected.

Belova E., M. Kawnine, I. Häggström, T. Sergienko, S. Kirkwood, and A. Tjulin, "Tristatic observation of polar mesosphere winter echoes with the EISCAT VHF radar on 8 January 2014: a case study", Earth, Planets and Space, 70, 110, doi:10.1186/s40623-018-0878-5, 2018.

Depletion of mesospheric sodium during extended period of pulsating aurora

The Na density depletion due to charge transfer reactions between Na atoms and molecular ions produced by high-energy electron precipitation during a pulsating aurora (PsA) was quantitatively evaluated. An extended period of PsA was captured by an all-sky camera at the European Incoherent Scatter (EISCAT) radar Tromsø site (69.6°N, 19.2°E) during a 2 h interval from 00:00 UT to 02:00 UT on 25 January 2012. During this period, using the EISCAT very high frequency (VHF) radar, we detected three intervals of intense ionization below 100 km that were probably caused by precipitation of high-energy electrons during the PsA (Figure 12). In these intervals, the sodium lidar at Tromsø observed characteristic depletion of Na density at altitudes from 97 km to

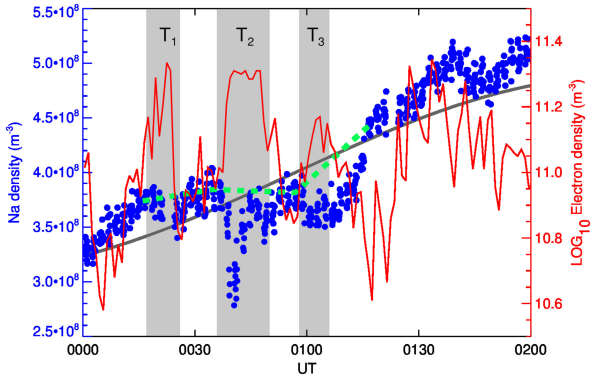

Figure 12: Mean Na and electron density from 97 km to 100 km. Na density and electron density variations are indicated by blue dots and red lines, respectively. Temporal resolution for Na density is 5 s. Gray line shows wave component with 6 h period proved by the Lomb-Scargle method. The bright green dashed line shows background variation in Na density for time interval T_1, T_2, and T_3.

100 km. These Na density depletions lasted for 8 min and represented 5 % to 8 % of the background Na layer. To examine the cause of this depletion, we modeled the depletion rate based on charge transfer reactions with NO^+ and O_2^+ while changing the R value which is defined as the ratio of NO^+ to O_2^+ densities, from 1 to 10. The correlation coefficients between observed and modeled Na density depletion calculated with typical value $R = 3$ for time intervals T_1, T_2, and T_3 were 0.66, 0.80 and 0.67, respectively. The observed Na density depletion rates fall within the range of modeled depletion rate calculated with R from 1 to 10. This suggests that the charge transfer reactions triggered by the auroral impact ionization at low altitudes are the predominant process responsible for Na density depletion during PsA intervals.

Takahashi, T., K. Hosokawa, S. Nozawa, T. T. Tsuda, Y. Hiraki, J. Sakai, Y. Ogawa, M. Tsutsumi, H. Fujiwara, T. D. Kawahara, N. Saito, S. Wada, T. Kawabata, and C. Hall, "Depletion of mesospheric sodium during extended period of pulsating aurora", J. Geophys. Res., doi:10.1002/2016JA023472, 2017.

GPS scintillations associated with cusp dynamics and polar cap patches

Jin et al. investigated the relative scintillation levels associated with cusp dynamics (including precipitation, flow shears, etc.) with and without the formation of polar cap patches (PCPs) around the cusp inflow region. The ESR data were utilised to identify time periods both with and without PCPs as well as gain an understanding as to dynamical processes occurring in the cusp region (eg flow shears, auroral particle precipitation). These data were combined with data from two GPS scintillation receivers located on Svalbard. Instances of PCPs which occurred with significant auroral dynamics were associated with a significantly higher GPS phase scintillation level (up to 0.6 rad) than those observed for the other two alternatives, i.e., cusp dynamics without PCPs, and PCPs without cusp aurora. The authors concluded that the worst global navigation satellite system space weather events on the dayside occur when polar cap patches enter the polar cap and are subject to particle precipitation and flow shears, which is analogous to the nightside when polar cap patches exit the polar cap and enter the auroral oval. Figure 13 indicates the two time periods used in the study and show the location of the ESR in both the pre- and post-noon MLT sector (panels a and b), along with ESR 42 m data indicating the ionospheric conditions (panels d to g).

Jin, Y., J. I. Moen, K. Oksavik, A. Spicher, L. B. N. Clausen, and W. J. Miloch, "GPS scintillations associated with cusp dynamics and polar cap patches", Journal of Space Weather and Space Climate, 7, A23, doi:10.1051/swsc/2017022, 2017.

David et al. used the long-run data taken during the International Polar Year (IPY) by the ESR in 2007 to study ionospheric upflow events. They set a lower limit of flux of $10^{13}\,m^{-2}s^{-1}$, and classified the upflow events into three categories depending on their upflow flux. They found that contrary to previous observations, there is a greater occurrence of upflow around noon during highly disturbed conditions than for moderate conditions. The seasonal distribution revealed that it is the high flux that shows a preference for noon in the summer at high geomagnetic activity; the low-flux upflow is broadly distributed across all seasons, activity levels and times of day.

David, T. W., D. M. Wright, S. E. Milan, S. W. H. Cowley, J. A. Davies, I. McCrea, "A study of observations of ionospheric upwelling made by the EISCAT Svalbard Radar during the International Polar Year campaign of 2007", Journal of Geophysical Research: Space Physics, 123, doi:10.1002/2017JA024802, 2018.

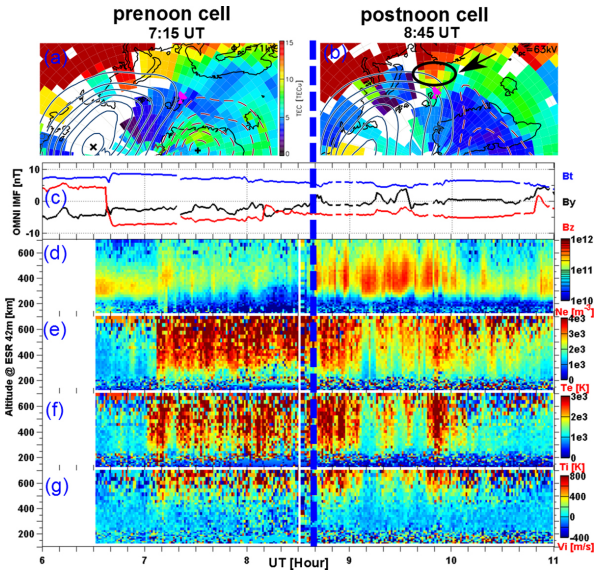

Figure 13: Event overview on 3 December, 2011. (a, b) The GPS TEC maps at 7:15 UT and 8:45 UT, respectively. The ESR location is indicated by a pink radar symbol above Svalbard. (b) The high density plasma moved poleward toward the Svalbard archipelago and it is annotated by a black circle and a black arrow. (c) The total magnetic field (B_t), B_y and B_z component of IMF from the OMNI dataset. (d–g) The electron density (N_e), electron temperature (T_e), ion temperature (T_i), and line of sight ion velocity (V_i) as measured by the ESR 42 m antenna. The vertical dashed blue line delimits the prenoon and postnoon sectors.

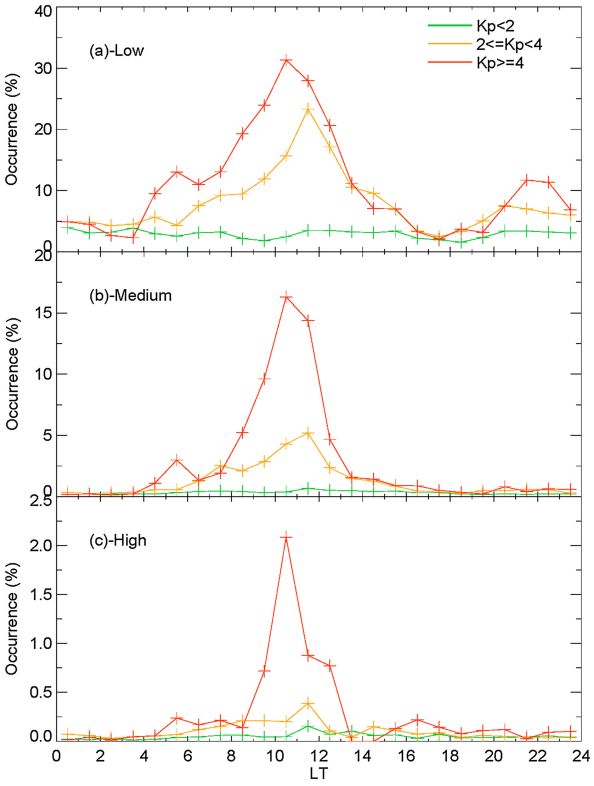

Figure 14: The local time distribution of upflow occurrence for low, medium and high flux events. The data are separated by K_p as a proxy for geomagnetic activity.

Statistical study about the influence of particle precipitation on mesosphere summer echoes in polar latitudes during July 2013

In the absence of particle precipitation on 8–12 July, 2013, PMSE observed at EISCAT VHF indicates that particle precipitation is not a necessary condition for PMSE. Even so, particle precipitation still affects PMSE when they both occur simultaneously. The relationship between PMSE and particle precipitation both represented by average electron density, occurring simultaneously for time interval of various lengths ($t \geq 2.56\,\mathrm{min}$), is statistically analyzed using the Spearman rank and Pearson linear correlation coefficients. By comparing the average electron density at altitude of 90 km (proxy of particle precipitation) and PMSE region at altitude of 80 km to 90 km (proxy of PMSE), the new method may compare the two phenomena directly and give some relationship between them. The percentage of events having positive values is dominant (Figure 15), which shows that the electron density variations due to the ionization produced by energetic particle precipitations might have some relationship with PMSE intensity. Moreover, the small percentage of negative correlation coefficient observed might be caused by the very strong precipitation at that time.

Abdur Rauf, Hailong Li, Safi Ullah, Lin Meng, Bin Wang and Maoyan Wang, "Statistical study about the influence of particle precipitation on mesosphere summer echoes in polar latitudes during July 2013", Earth, Planets and Space, 70, 108, doi:10.1186/s40623-018-0885-6, 2018.

Auroral molecular-emission effects on the atomic oxygen line at 777.4 nm

One of the representative auroral emission lines that radiates from F-region heights and is measurable on the ground is the 777.4 nm line from excited atomic oxygen. This line has been adopted, along with another E-region emission line, for ex-

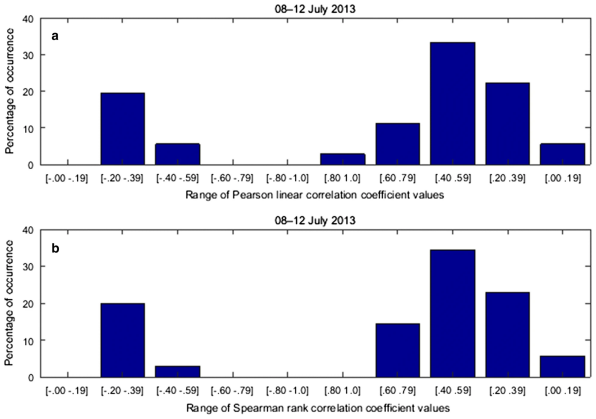

Figure 15: Percentage of occurrence of different ranges of Pearson linear correlation coefficient (a) and Spearman rank correlation coefficient (b) for all events in the 5-day campaign.

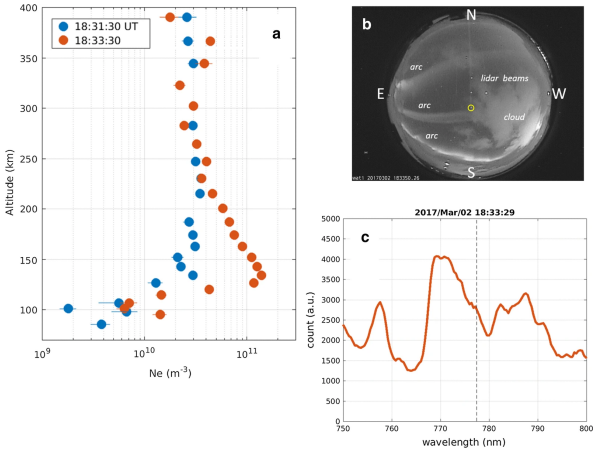

Figure 16: (a) Height profiles of the EISCAT-measured electron density at 18:31:30 UT (blue) and 18:33:30 UT (orange) on 2 March 2017. Measurement uncertainty of ± 1 $sigma$ is marked by a horizontal bar in each color. (b) An image from the Tromsø all-sky camera, which was taken at 18:33:50 UT. The direction of the EISCAT radar and spectrograph measurements is marked by a yellow circle. Five faint lines from the northern edge represent contaminations of a sodium lidar. (c) Spectrum measured at 18:33:29 UT on 2 March 2017, at wavelength of 750 nm to 800 nm. A vertical dashed line is marked at 777.4 nm.

ample 427.8 nm, to estimate the mean energy and total energy flux of precipitating auroral electrons. The influence of emissions from part of the molecular nitrogen band, which mainly radiate from E-region heights, should be carefully evaluated because it might overlap the 777.4 nm atomic oxygen line in the spectrum (Figure 16). We performed statistical analysis of auroral spectrograph measurements that were obtained during the winter of 2016–2017 in Tromsø, Norway, to derive the ratio of the intensity of the 777.4 nm atomic oxygen line to that of the net measurement through a typically used optical filter with a full width at half maximum of a few nm. The ratio had a negative trend against geomagnetic activity, with a primary distribution of 0.5 to 0.7 and a minimum value of 0.3 for the most active auroral condition in this study. This result suggests that the 30 % to 50 % emission intensities measured through the optical filter may be from the molecular nitrogen band.

Oyama, S., T. T. Tsuda, K. Hosokawa, Y. Ogawa, Y. Miyoshi, S. Kurita, A. E. Kero, R. Fujii, Y. Tanaka, A. Mizuno, T. Kawabata, B. Gustavsson, T. Leyser, "Auroral molecular-emission effects on the atomic oxygen line at 777.4 nm", Earth Planets Space, 70:166, doi:10.1186/s40623-018-0936-z, 2018.

Seasonal and solar cycle variations of thermally excited 630.0 nm emissions in the polar ionosphere

Kwagala et al. looked at solar cycle and seasonal variations in strong, thermally excited 630.0 nm emissions in the polar ionosphere. 15 years of electron temperature (T_e) and density measurements (N_e) (from 2000 to 2015) from the EISCAT Svalbard 42 m Radar were used to derive the thermal emission intensity. Thermally excited emissions were found to maximize at solar maximum with peak occurrence rate of around 40 % compared to around 2 % at solar minimum. These emissions also have the highest occurrence in equinox and the lowest occurrence rate in summer and winter. There is an equinoctial asymmetry in the occurrence rate which reverses with the solar cycle. This equinoctial asymmetry is attributed to variations of the solar wind-magnetosphere coupling arising from the Russell-McPherron effect. The occurrence rate of thermal excitation emission on the dayside, at Svalbard, has been found to be higher in autumn than spring at solar maximum and the reverse at solar minimum. Enhanced electron temperatures characterize the strong thermal component for solar minimum and winter, whereas enhanced electron densities characterize the thermal component for solar maximum. Figure 17 shows electron density (panels a and c) and electron temperature (panels b and d) associated with the strong thermal component, for both Solar minimum (panels a and b), and Solar Maximum (panels c and d) where the T_e (solar min) and N_e (solar

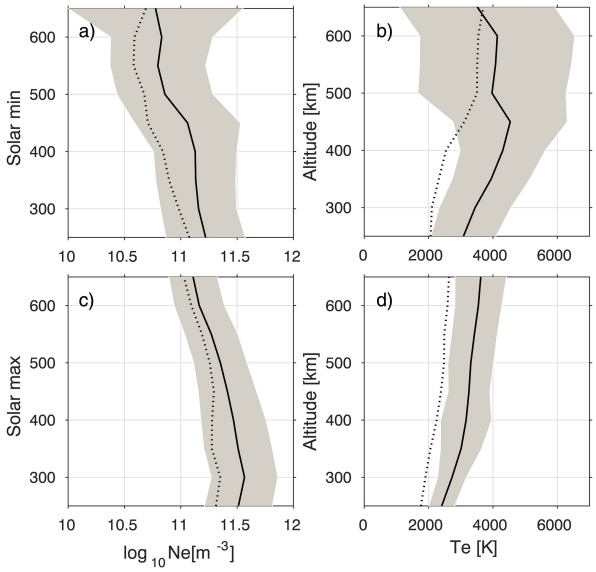

Figure 17: Distribution of electron temperature (b,d) and electron density (a,c) for solar minimum (a,b) and solar maximum (c,d), associated with the strong thermal component. The black line shows the strong thermal average with the gray shading marking the standard deviation of the strong thermal distribution. The dotted line shows the solar minimum/maximum mean for reference.

max) dominance can be seen. The results point to solar wind-magnetosphere-ionosphere coupling as the dominant controlling process.

Kwagala, N. K., K. Oksavik, D. A. Lorentzen, M. G. Johnsen, K. M. Laundal, "Seasonal and Solar Cycle Variations of Thermally Excited 630.0 nm Emissions in the Polar Ionosphere", Journal of geophysical research: Space physics, 123(8), 7029–7039, doi:10.1029/2018JA025477, 2018.

Plasma line observations from the EISCAT Svalbard Radar during the International Polar Year

Photo-electrons and secondary electrons from particle precipitation enhance the incoherent scatter plasma line to levels sufficient for detection. When detectable the plasma line gives accurate measure of the electron density and can potentially be used to constrain incoherent scatter estimates of electron temperature. Examined was the statistical occurrence of plasma line enhancements with data from the high-latitude EISCAT Svalbard Radar obtained during the International Polar Year (IPY, 2007–2008), shown in Figure 18. A computationally fast method was implemented to recover the range-frequency dependence of the plasma line. Plasma line backscatter strength strongly depends on time of day, season, altitude, and geomagnetic activity, and the backscatter is detectable in 22.6 % of the total measurements during the IPY. As expected, maximum detection is achieved when photo-electrons due to the Sun's EUV radiation are present. During summer daytime hours the occurrence of detectable plasma lines at altitudes below the F-region peak is up to 90 %. During wintertime the occurrence is a few percent. Electron density profiles recovered from the plasma line show great detail of density variations in height and time. For example, effects of inertial gravity waves on the electron density are observed.

Ivchenko N., Nicola M. Schlatter, H. Dahlgren, Y. Ogawa, Yuka Sato, and Ingemar Häggström, "Plasma Line Observations from the EISCAT Svalbard Radar During the International Polar Year", Ann. Geophys., 35, 1143–1149, doi:10.5194/angeo-35-1143-2017, 2017.

Polar cap patches observed by the EISCAT Svalbard Radar: A statistical study of its dependence on the solar wind and IMF conditions

Polar cap patches are common irregularities in the polar ionosphere, where their formation and evolution can directly affect satellite navigations and communications as well as over-the-horizon radar observations, etc. However, affected by the various dynamic processes during the solar wind-magnetosphere-ionosphere coupling, there is no fully accepted formation mechanism of polar cap patches. In this study, a statistical analysis of 345 patches at the dayside sectors from 09:00 to 15:00 magnetic local time (MLT), observed by EISCAT Svalbard Radar (ESR) 42 m antenna from 2010 to 2013, has been performed. The dependence of their occurrence on solar wind and interplanetary magnetic field (IMF) conditions as well as their MLT distribution has been statistically investigated. The results show that the polar cap patches are preferentially formed during southward IMF conditions. In particular, the MLT dependence of the patches presents a clear IMF By-related prenoon-postnoon asymmetry, suggesting the patch formation is clearly modulated by the IMF By polarity. Moreover, the statistical results indicate that the patches should not be caused by the variations of the solar wind

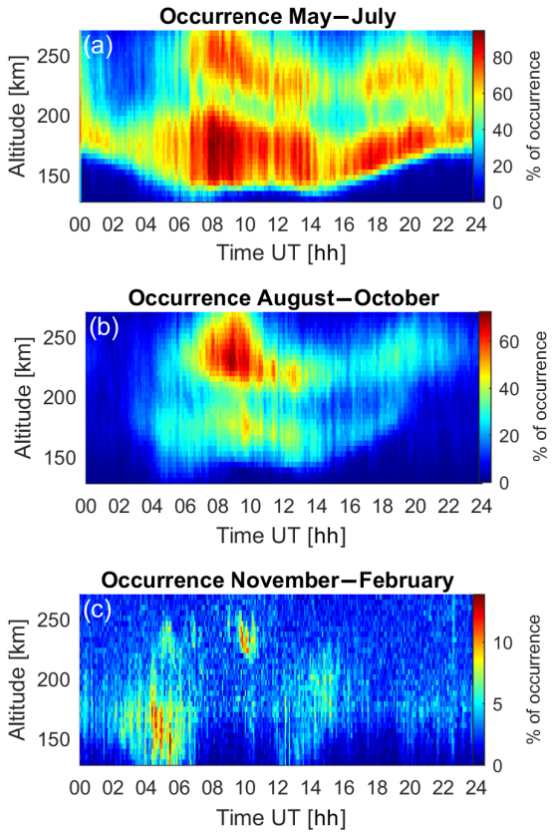

Figure 18: Occurrence of detected plasma line backscatter with 30 s integration: (a) May to July 2007; (b) August to October 2007; (c) November 2007 to February 2008. Magnetic local time at ESR is UT + 3.1 h.

dynamic pressure or the solar wind velocity. All the results indicate that the pulsed dayside magnetic reconnection is possibly a significant formation mechanism of polar cap patches.

Yuyan Jin, Zanyang Xing, Qinghe Zhang, Yong Wang, Yuzhang Ma, "Polar cap patches observed by the EISCAT Svalbard Radar: A statistical study of its dependence on the solar wind and IMF conditions", Journal of Atmospheric and Solar-Terrestrial Physics 192, doi:10.1016/j.jastp.2018.01.011, 2018.

Average field-aligned ion velocity over the EISCAT radars

Long-term measurements by the European Incoherent Scatter (EISCAT) radars at Tromsø (69.6°N, 19.2°E) and Svalbard (78.2°N, 16.0°E) are used to determine the climatology of the field-aligned ion velocity in the F region ionosphere (175 km to 475 km) at high latitudes. The average ion velocity is calculated at various altitudes and times of day. The magnitude of the average field-aligned ion velocity is on the order of 10 m/s, similar to previous results at middle and low latitudes. The results obtained for the two radars are in good agreement. During daytime the direction of the average field-aligned ion velocity changes from downward to upward around 350 km, while during nighttime it is upward at all heights. The reversal height of the daytime field-aligned ion velocity depends on solar activity. It is elevated by more than 100 km during high solar flux periods compared to low solar flux periods. The Thermosphere Ionosphere Electrodynamics General Circulation Model reproduces the main features of the field-aligned ion velocity climatology. The simulation results suggest that the plasma pressure gradient force and gravity force play a dominant role for the daytime field-aligned ion motion. The height pattern of the field-aligned ion velocity tends to be preserved in different solar activity conditions at constant pressure surfaces, but not at constant altitudes, which explains the observed dependence on solar activity. During nighttime, the effect of the neutral wind dominates the field-aligned ion velocity.

Yamazaki, Y., M. J. Kosch, and Y. Ogawa, "Average field-aligned ion velocity over the EISCAT radars". J. Geophys. Res., doi:10.1002/2017JA023974, 2017.

Equatorward propagating auroral arcs driven by ULF wave activity: Multipoint ground- and space-based observations in the dusk sector auroral oval

Baddeley et al. presented a rare occurrence of a prolonged sequence of equatorward moving arc structures in the dusk-side auroral oval over Svalbard. Simultaneous observations of the event were obtained from the ground based MSP at KHO and an All-Sky Camera (in Ny Ålesund), from the ESR, and from particle, magnetic field, and auroral emission instruments onboard the DMSP F16 satellite. Observations of temperature and density measurements from the ESR indicate significant joule heating effects adjacent to the arcs. The findings supports the interpretation of the arcs as resulting from a resonant wave structure on the Earth magnetic field generated by a compressional wave propagating earthward from the magnetotail. The detailed analysis provides the first direct assessment of the energy loss suffered by the wavefield due to both ionospheric heating and particle pre-

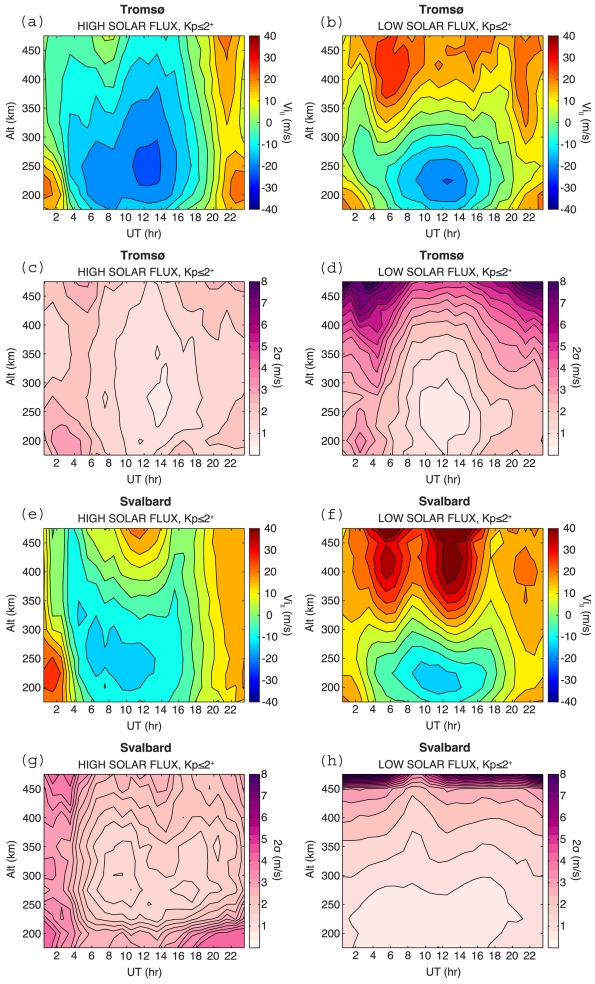

Figure 19: The dependence of the average field-aligned ion velocity (positive upward) on solar activity (a and b) for Tromsø and (e and f) for Svalbard. The 2σ errors are shown (c and d) for Tromsø and (g and h) for Svalbard. The average standard deviation is 21.7 m/s and 35.5 m/s for panels a and b, respectively, and 34.1 m/s and 38.7 m/s for panels e and f, respectively. The average 2σ error is 1.83 m/s and 3.14 m/s for panels a and b, respectively, and 2.44 m/s and 2.02 m/s for panels e and f, respectively.

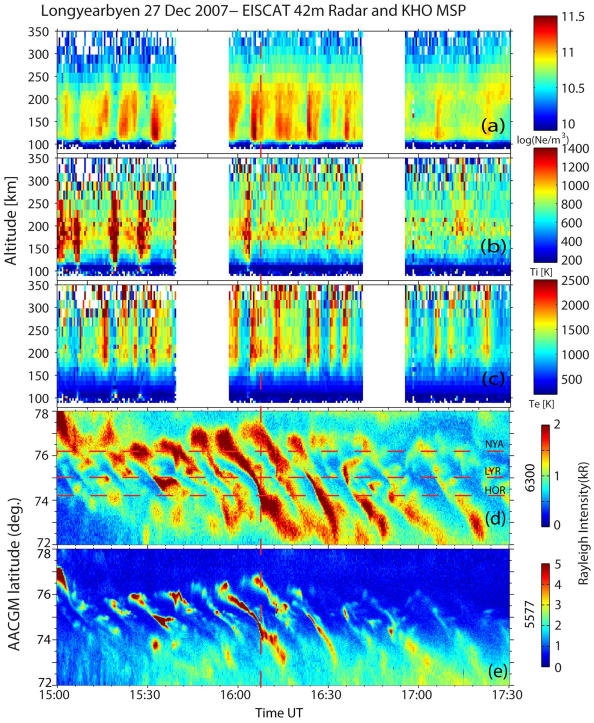

Figure 20: Ionospheric (a) electron density, (b) ion temperature (c) electron temperature measured by the ESR 42 m antenna. Auroral intensities in the (d) 630.0 nm and (e) 557.7 nm wavelengths as measured by the MSP. The red horizontal dashed lines in panel (d) mark the positions of NYA, LYR (also the pointing direction of the ESR 42 m beam on the MSP field of view) and HOR. The red vertical dashed line indicates the time of the DMSP F16 satellite conjunction.

cipitation. Figure 20 shows data from the ESR (panels a to c) and the co-located MSP (panels d and e). The horizontal dashed lines in panel d indicate the latitude of the ground magnetometers (NYA, LYR and HOR) and the ESR (LYR). It can be seen that as the arc passes over LYR, there is a large increase in electron density and temperature, whereas in between the arcs there is significant increase in ion temperature.

Baddeley, L. J., D. A. Lorentzen, N. Partamies, W. Denig, V. A. Pilipenko, K. Oksavik, X.-C. Chen and Y. Zhang, "Equatorward Propagating Auroral Arcs driven by ULF Wave Activity: Multipoint Ground and Space based Observations in the Dusk Sector Auroral Oval", J. Geophys. Res. Space Physics, 122, doi:10.1002/2016JA023427, 2017.

Ionospheric response observed by EISCAT during the 6–8 September 2017 space weather event

The EISCAT radars in Tromsø and on Svalbard observed ionospheric plasma conditions covering 68° to 81° geomagnetic latitude, during 6–8 September 2017, shown in Figure 21. This is a period when X2.2 and X9.3 X-ray flares occurred, two interplanetary coronal mass ejections (ICMEs) arrived at the Earth accompanied by enhancements of MeV-range energetic particle flux in both the solar wind (SEP event) and inner magnetosphere, and an AL < -2000 substorm took

place. (1) Both X flares caused enhancement of ionospheric electron density for about 10 min. The X9.3 flare also increased temperatures of both electrons and ions over 69° to 75° geomagnetic latitude until the X-ray flux decreased below the level of X-class flares. However, the temperature was not enhanced after the previous X2.2 flare in the prenoon sector. (2) At around 75° geomagnetic latitude, the prenoon ion upflow flux slightly increased the day after the X9.3 flare, which is also after the first ICME and a SEP event, while no outstanding enhancement was found at the time of these X flares. (3) The upflow velocity sometimes decreased when the interplanetary magnetic field (IMF) turned southward. (4) Before the first ICME arrival after the SEP event under weak IMF with B_z around 0 nT, a substorm-like expansion of the auroral arc signature took place without local geomagnetic signature near local midnight, while no notable change was observed after the ICME arrival. (5) AL reached bwlow −2000 nT only after the arrival of the second ICME with strongly southward IMF. Causality connections between the solar/solar wind event and the ionospheric responses remain unclear.

Yamauchi, M., Sergienko, T., Enell, C.-F., Schillings, A., Slapak, R., Johnsen, M. G., et al., "Ionospheric response observed by EISCAT during the 6–8 September 2017 space weather event: Overview", Space Weather, 16, 1437–1450. doi:10.1029/2018SW001937, 2018.

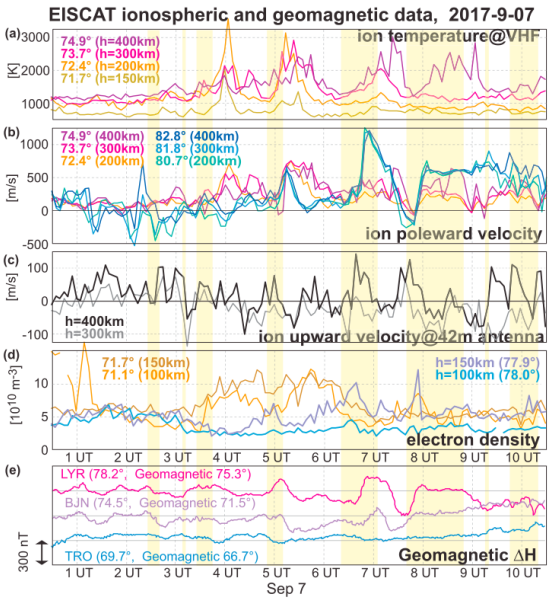

Figure 21: Line plots of (a) T_i data from the Tromsø VHF radar, (b) V_i data from the Tromsø VHF radar and the Svalbard 32 m antenna, (c) V_i data from the Svalbard 42 m antenna, and (d) N_e data from the Tromsø VHF radar and the Svalbard 42 m antenna, for selected altitudes and limited time periods. (e) Plot of geomagnetic horizontal (H) deviation. LYR = Longyearbyen geomagnetic station; BJN = Bear Island geomagnetic station; TRO = Tromsø geomagnetic station.

Active experiments

The behavior of electron density and temperature during ionospheric heating near the fifth electron gyrofrequency

The experimental phenomena involving the changes in electron temperature and electron density as a function of pump frequency during an ionospheric heating campaign at EISCAT near Tromsø, Norway, are studied. When the pump frequency is slightly above the fifth electron gyrofrequency, the UHF radar observation shows some apparent enhancements over a wide altitude range in radar echo, ion line and electron density respectively, which are apparently altitude independent and consistent temporally with the up-shifting and spread of plasma line around the reflection altitude (Figure 22). However, they do not in fact correspond to true increase in electron density. Based on some existing theories, some discussions are presented to try to explain the above enhancements and the up-shifting and spread of plasma line. Even so, the mechanism remains to be determined.

Wu, J., Wu, J., Rietveld, M. T., Haggstrom, I., Zhao, H., and Xu, Z., "The behavior of electron density and temperature during ionospheric heating near the fifth electron gyrofrequency", J. Geophys. Res. Space Physics, 122, 1277–1295, doi:10.1002/2016JA023121, 2017.

Results of ionospheric heating experiments involving an enhancement in electron density in the high latitude ionosphere

The observation of Ultra High Frequency radar during an ionospheric heating experiment carried out at Tromsø site of EISCAT, Norway, is analyzed. When pump is operating slightly above the fifth electron gyrofrequency, some strong enhancements in radar echo and electron density occur in a wide altitude range and are in sync with the shifting and spread of plasma line around the reflec-

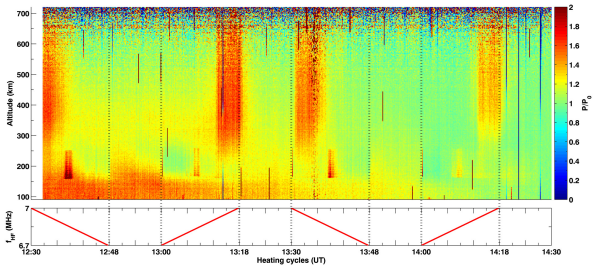

Figure 22: The ratios of UHF radar echo power from the undecoded 640 µs alternating code pulse with a height resolution of 94 km for 12.5° zenith versus heating cycles, where the black dotted vertical lines correspond to heating on and off and the red solid line the stepping change in pump frequency.

tion altitude, which may be due to the focusing or collimating of radar wave by irregularities

Wu Jun, Wu Jian, and Xu Zhengwen, "Results of Ionospheric Heating Experiments Involving an Enhancement in Electron Density in the High Latitude Ionosphere", Plasma Sci. Technol. 18(9), doi:10.1088/1009-0630/18/9/03, 2016.

Survey of conditions for artificial aurora experiments at EISCAT Tromsø using dynasonde data

We report a brief survey on conditions for artificial aurora optical experiments in F region heating with O-mode at the EISCAT Tromsø site using dynasonde data from 2000 to 2017 (Figure 23). The results obtained in our survey indicate the following: The possible conditions for conducting artificial aurora experiments are concentrated in twilight hours in both evening and morning, compared with late-night hours; the possible conditions appear in fall, winter, and spring, while there is no chance in summer, and the month-to-month variation among fall, winter, and spring is not clear. The year-to-year variation is well correlated with the solar cycle, and experiments during the solar minimum would be almost hopeless. These findings are useful for planning future artificial aurora optical experiments.

T. T. Tsuda, M. T. Rietveld, M. J. Kosch, S. Oyama, K. Hosokawa, S. Nozawa, T. Kawabata, A. Mizuno and Y. Ogawa, "Survey of conditions for artificial aurora experiments at EISCAT Tromsø using dynasonde data", Earth, Planets and Space, 70:40, doi:10.1186/s40623-018-0805-9, 2018.

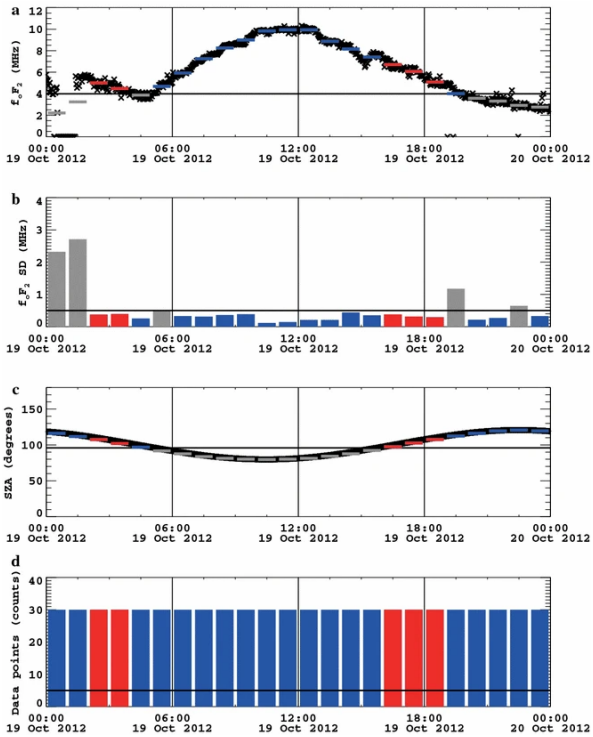

Figure 23: (a) Variation in foF2 measured with EISCAT dynasonde in Tromsø on 19 October, 2012. The black horizontal line corresponds to the threshold, i.e., 4 MHz. The shorter horizontal lines represent the averaged values for each hour. (b) Variation in one standard deviation (SD) of foF2 for each hour. The black horizontal line corresponds to the threshold, i.e., 0.5 MHz. (c) Variation in the solar zenith angle (SZA). The black horizontal line corresponds to the threshold, i.e., 96°. The shorter horizontal lines represent the minimum values for each hour. (d) Variation in the number of foF2 data for each hour. The black horizontal line corresponds to the threshold, i.e., 5. Each value, which satisfied each threshold, is shown in blue, otherwise in gray. When all the four thresholds were satisfied at the same time, the values at that time are marked in red. Note that the time is written in UT (which is LT − 1 h (for winter time), at Tromsø).

The extending of observing altitudes of plasma and ion lines during ionospheric heating

The EISCAT UHF observation during an ionospheric heating experiment on 11 March 2014 illustrated a remarkable extension of observing altitudes of HFPL and HFIL (Figure 24), implying that the enhanced Langmuir and ion acoustic waves should satisfy the Bragg condition within the extending altitude range. An analysis shows that the

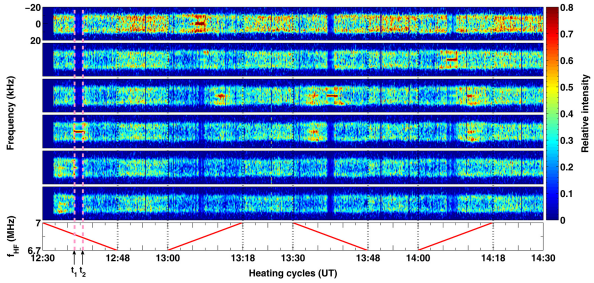

Figure 24: The ion lines at altitudes of (first panel) 215.43 km, (second panel) 212.5 km, (third panel) 209.57 km, (fourth panel) 206.63 km, (fifth panel) 203.7 km, and (sixth panel) 200.77 km versus (seventh panel) heating cycles.

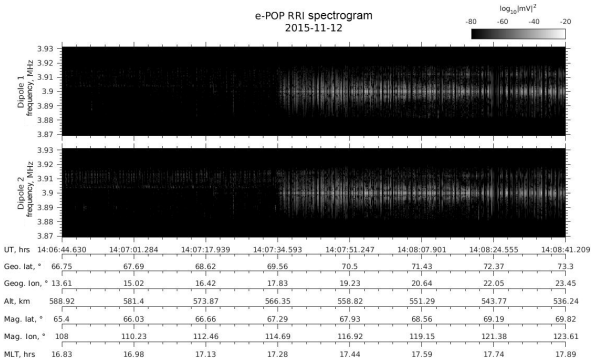

Figure 25: Overview of the detected voltage on the two antenna dipoles for the CASSIOPE passage over EISCAT Heating from 14:06:44.630 UT to 14:08:41.209 UT on 12 November 2015. The RRI was pre-programmed to sweep between 13 different frequency bands, one of which contained the Heating signal at $f_0 = 3.900\,\mathrm{MHz}$. The panels show the signal level in the 60 kHz wide frequency band around the Heating signal at f_0, which can be seen from about 14:07:34 UT.

dependence of wave number of the enhanced ion acoustic wave on the profiles of enhanced electron temperature and ion mass, leads to the extension of observing altitudes of HFIL. The altitude extension of HFPL is dependent mainly on the profile of the electron density, although it is not independent of the profile of the electron temperature.

Jun Wu, Jian Wu, M. T. Rietveld, I. Haggstrom, Haisheng Zhao and Zhengwen Xu, "The Extending of Observing Altitudes of Plasma and Ion Lines During Ionospheric Heating", J. Geophys. Res. Space Physics, 123(11), doi:10.1002/2017JA024809, 2018.

Evidence of L-mode electromagnetic wave pumping of ionospheric plasma near geomagnetic zenith

The response of ionospheric plasma to pumping by powerful HF (high frequency) electromagnetic waves transmitted from the ground into the ionosphere is the strongest in the direction of geomagnetic zenith. We present experimental results from transmitting a left-handed circularly polarized HF beam from the EISCAT (European Incoherent SCATter association) Heating facility in magnetic zenith. The CASSIOPE (CAScade, Smallsat and IOnospheric Polar Explorer) spacecraft in the topside ionosphere above the F-region density peak detected transionospheric pump radiation (Figure 25), although the pump frequency was below the maximum ionospheric plasma frequency. The pump wave is deduced to arrive at CASSIOPE through L-mode propagation and associated double (O to Z, Z to O) conversion in pump-induced radio windows. L-mode propagation allows the pump wave to reach higher plasma densities and higher ionospheric altitudes than O-mode propagation so that a pump wave in the L-mode can facilitate excitation of upper hybrid phenomena localized in density depletions in a larger altitude range. L-mode propagation is therefore suggested to be important in explaining the magnetic zenith effect.

Leyser T. B., H. Gordon James, B. Gustavsson, and M. T. Rietveld, "Evidence of L-mode electromagnetic wave pumping of ionospheric plasma near geomagnetic zenith", Ann. Geophys., 36, 243–251, doi:10.5194/angeo-36-243-2018, 2018.

Systematic variation in observing altitude of enhanced ion line by the pump near fifth gyroharmonic

The observation at EISCAT UHF demonstrated a systematic variation in the altitude of HFIL, which is quite remarkably dependent on the pump frequency. The analysis shows that the systematic variation in the altitude of HFIL is principally dependent on the enhanced electron temperature, although the changes in the profile of the electron density brought about by the ionospheric heating are not independent of those systematic altitude variations.

Jun Wu, Jian Wu, M. T. Rietveld, I. Haggstrom, Haisheng Zhao, Tong Xu and Zhengwen Xu, "Systematic variation in observing altitude of enhanced ion line by the pump near fifth gyroharmonic", Plasma Sci. Technol. 20, 125301, doi:10.1088/2058-6272/aadd44, 2018.

First observations of recurring HF enhanced topside ion line spectra near the fourth gyroharmonic

Rexer et al. presented the first incoherent scatter radar observations of systematically recurring, high-frequency (HF)-enhanced ion line spectra at the topside F-region ionosphere, during magnetic field aligned HF pumping in an O-mode polarization. The EISCAT UHF radar was directed in magnetic zenith, while the EISCAT heater pump frequency was stepped across the double resonance of the fourth harmonic of the electron gyrofrequency and the local upper hybrid frequency, in a 3 min-on, 3 min-off pump cycle. Topside and bottomside enhancements occurred at the respective plasma resonance altitude and seemed to be asymmetrically conditioned by the relative proximity of the pump frequency to the double resonance frequency. The topside HF-induced ion line (THFIL) enhancements predominantly appeared while the pump frequency was just below the double resonance frequency and only simultaneous to strong bottomside HF-induced ion line (BHFIL) enhancements. A powerful, O-mode HF radio wave, transmitted in the direction of magnetic zenith is reflected a few kilometers below the plasma resonance altitude, where the pump frequency is equal to the local plasma frequency, on the bottomside F-region in the ionosphere. The enhancements present evidence of radio wave propagation outside the standard radio window, or Spitze angle, which at Tromsø is around 6°. The Spitze angle is defined as the angle of incidence for which an O-mode wave, transmitted from the ground, has refracted to being magnetic field aligned ($\vec{k} \parallel \vec{B}_0$) when reaching the plasma resonance height. The authors considered a variety of mechanisms to explain this phenomena and suggest this propagation outside the radio window could be facilitated by density striations in the plasma. Figure 26 shows a summary of the enhancements observed in the ion line backscatter power relative to the difference of the pump and double resonance frequency. Topside enhancements are shown in orange while bottomside enhancements are shown in purple. The superposed lines show the mean of the observation. Negative values indicate an HF pump just below the double resonance frequency. It can be seen that as the HF pump frequency is increased throughout the pulse the BHFIL intensity increase until they reach a maximum and decrease significantly, then disappear completely. Simultaneous to the increase in the BHFIL clear enhancements at the topside ionosphere are observed and the strongest backscatter from the THFIL coincides with the strongest backscatter from the BHFIL.

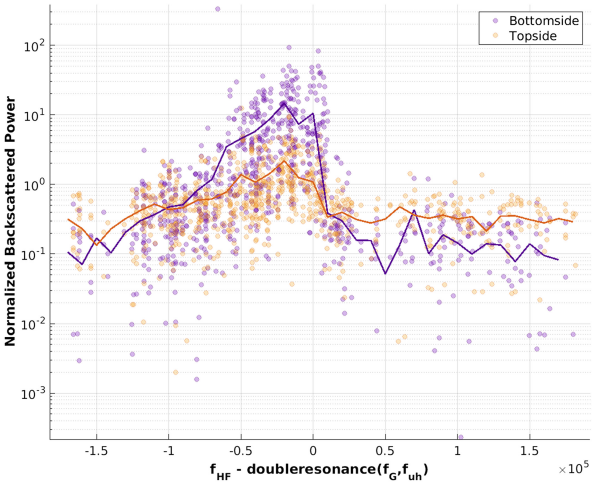

Figure 26: Comparison of all 33 heating pulses. Backscattered ion line power relative to the difference of the pump and double resonance frequency. Topside enhancements are shown in orange while bottomside enhancements are shown in purple. The superposed lines show the mean of the observation.

Rexer, T., B. Gustavsson, T. Leyser, M. Rietveld, T. Yeoman, T. Grydeland, "First observations of recurring HF enhanced topside ion line spectra near the fourth gyroharmonic", Journal of Geophysical Research: Space Physics, 123, 8649–8663, doi:10.1029/2018JA025822, 2018.

The polarization characteristics of ELF/VLF waves generated via HF heating experiments of the ionosphere by EISCAT

The frequency characteristics of ELF/VLF radiation sources in the amplitude modulated (AM) and dual-beam beat-wave (BW) modes are compared, and the polarization of the horizontal ELF/VLF magnetic field received at 15 km from the heating facility is studied. The results show that in the AM mode, the amplitude of the ELF/VLF signal decreases as the increase in radiation frequency when the amplitude of the ELF/VLF signal reaches the maximum at 2017 Hz. In the BW mode, the maximum appears at 2017 Hz, but the overall amplitude of the ELF/VLF signal increases as the increase in radiation frequency. The AM and BW modes have

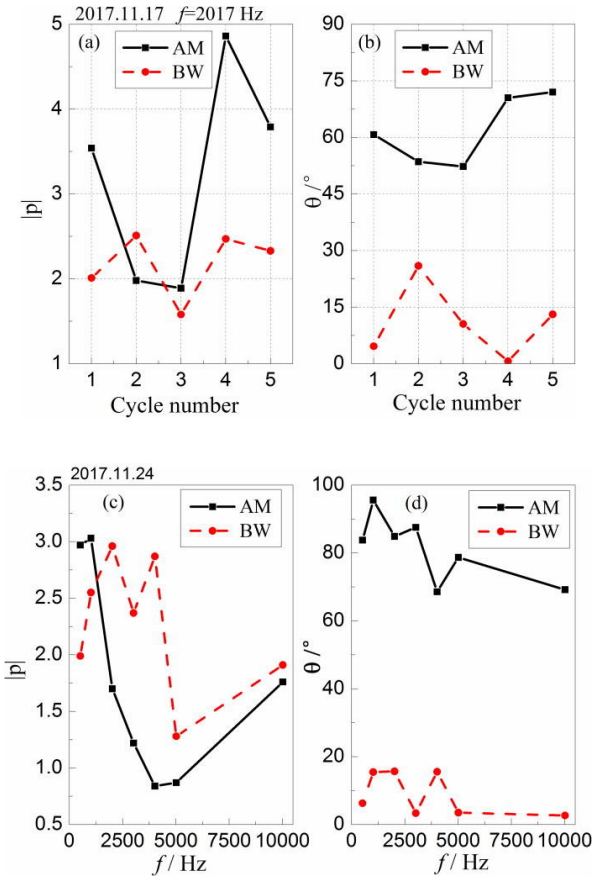

Figure 27: Two of the experimental results for the polarization factors $|p|$ and θ. (a) and (b) display data from 17 November 2017, and (c) and (d) data from 24 November 2017.

different frequency characteristics on ELF/VLF radiation sources formed by modulation and heating of the ionosphere. When the frequency is low, the amplitude of the ELF/VLF signal excited by the AM mode is greater than that excited by the BW mode, but as the frequency increases, the BW mode performs better than the AM mode. Under the same background conditions, the polarization characteristics of the ELF/VLF radiation signals excited by the AM and BW modes are different (Figure 27). The former tends to produce circularly polarized waves, while the latter produces linearly polarized waves.

Jutao Yang, Qingliang Li, Jianguo Wang, Shuji Hao, and Guanglin Ma, "The polarization characteristics of ELF/VLF waves generated via HF heating experiments of the ionosphere by EISCAT", Physics of Plasmas, 25, 092902, doi:10.1063/1.5044611, 2018.

Threshold of parametric instability in the ionospheric heating experiments

Many observations in the ionospheric heating is attributed to parametric instability (PI). The general dispersion relation and the threshold of PI are derived by considering the inhomogeneous spatial distribution of pump wave field. It is shown that the threshold of PI is influenced by the effective electron and ion collision frequencies and the pump wave frequency. Both collision and Landau damping should be considered in the PI calculation. The derived threshold expression has been used to calculate the required threshold of PI for several ionospheric conditions during heating experiments conducted employing EISCAT heater in Tromsø, Norway, on 2 October 1998, 8 November 2001, 19 October 2012 and 7 July 2014. The results indicate that the calculated threshold is in good agreement with the experimental observations.

Xiang Wang, Chen Zhou, Moran Liu, Farideh Honary, Binbin Ni and Zhengyu Zhao, "Threshold of parametric instability in the ionospheric heating experiments", Plasma Sci. Technol. 20, 115301, doi:10.1088/2058-6272/aac71d, 2018.

Method developments

Electron density inversed by plasma lines induced by suprathermal electron in the ionospheric modification experiment

The plasma lines are not routinely detected by ISR due to the low intensity, which falls below the measured spectral noise level. However, the plasma lines are occasionally enhanced by suprathermal electrons through the Landau damping and detectable to ISR. The enhanced plasma line by pump may be considered as manifest of the suprathermal electrons. The electron density profile is also obtained from HFPL. This study can be a potential technique for obtaining the electron density during ionospheric heating.

Xiang Wang and Chen Zhou, "Electron density inversed by plasma lines induced by suprathermal electron in the ionospheric modification experiment", Advances in Space Research, 61(9), doi:10.1016/j.asr.2018.02.001, 2018.

Background suppression and strong phase codes in incoherent scatter lag profile inversion

The near-perfect radar codes for lag profile inversion, which include e.g. the multi-purpose radar modulations, have been optimised without taking into account the effect of the receiver impulse response. While arbitrary transmitter modulations can be analysed with lag profile inversion, this requires that the transmitted waveform is sampled with a very high sample rate or shape of the elementary pulses is otherwise known. In this paper the concept of strong phase codes, which was originally developed for the alternating codes, is shown to work with the near-perfect radar codes. When the optimised code cycle is transmitted twice, with the sign of every second bit swapped in the second transmission cycle, one can safely sample the transmitted waveform with a sample rate matched to the modulation bit length. Just like in decoding of strong alternating codes, the range sidelobes generated in decoding of the first and the second code cycle will exactly cancel out. The alternating codes have also the very beneficial property that their decoding will exactly cancel out a DC offset in the radar receiver. The near-perfect codes do not have this property, but the lag profile inversion technique was modified to include also background suppression. Effect of the background suppression to the statistical accuracy of the final decoded lag profiles was shown to be negligible.

I. I. Virtanen, "Background Suppression and Strong Phase Codes in Incoherent Scatter Lag Profile Inversion", IEEE Geoscience and Remote Sensing Letters 12(4), 841–845, doi:10.1109/LGRS.2014.2363692, 2015.

Publications 2017

Akbari, H., A. Bhatt, C. La Hoz, J. Semeter, "Incoherent Scatter Plasma Lines: Observations and Applications", Space Sci. Rev., doi:10.1007/s11214-017-0355-7, 2017

Baddeley, L. J., D. A. Lorentzen, N. Partamies, M. Denig, V. A. Pilipenko, K. Oksavik, X. Chen, Y. Zhang, "Equatorward propagating auroral arcs driven by ULF wave activity: Multipoint ground- and space-based observations in the dusk sector auroral oval", J. Geophys. Res. Space Physics, 122, doi:10.1002/2016JA023427, 2017

Belehaki, A., M. Hapgood, J. Watermann, "Access to data from near-Earth space", DOI:10.1051/978-2-7598-1949-2, ISBN: 978-2-7598-1949-2, 174 pages, 2017

Bjoland, L. M., Y. Ogawa, C. Hall, M. Rietveld, U. P. Løvhaug, C. La Hoz, H. Miyaoka, "Long-term variations and trends in the polar E-region", Journal of Atmospheric and Solar-Terrestrial Physics, 163, 85-90, 2017

Blagoveshchenskaya, N. F., T. D. Borisova, A. S. Kalishin, T. K. Yeoman, I. Häggström, "First observations of electron gyro-harmonic effects under X-mode HF pumping the high latitude ionospheric F-region", Journal of Atmospheric and Solar-Terrestrial Physics, 155, 36-49, doi.org/10.1016/j.jastp.2017.02.003, 2017

Blagoveshchenskaya, N. F., T. D. Borisova, T. K. Yeoman, "Comment on "Parametric instability induced by X-mode wave heating at EISCAT" by Wang et al. (2016)", Journal of Geophysical Research: Space Physics, 122, 12,570–12,585, doi.org/10.1002/2017JA023880, 2017

Borisova, T. D., N. F. Blagoveshchenskaya, T. K. Yeoman, I. Häggström, "Excitation of Artificial Ionospheric Turbulence in the High-Latitude Ionospheric F Region as a Function of the EISCAT/Heating Effective Radiated Power", Radiophysics and Quantum Electronics, 60, 4, DOI 10.1007/s11141-017-9798-7, 2017

Dahlgren, H., N. M. Schlatter, N. Ivchenko, L. Roth, A. Karlsson, "Relation of anomalous F region radar echoes in the high-latitude ionosphere to auroral precipitation", Ann. Geophysicae, 35, 475-479, doi:10.5194/angeo-35-475-2017, 2017

Dahlgren, H., B. S. Lanchester, N. Ivchenko, D. K. Whiter, "Variations in energy, flux, and brightness of pulsating aurora measured at high time resolution", Ann. Geophysicae, 35, 493-503, doi:10.5194/angeo-35-493-2017, 2017

Forte, B., C. Coleman, S. Skone, I. Häggström, C. Mitchell, J. Kinrade, G. Bust, "Identification of scintillation signatures on GPS signals originating from plasma structures detected with EISCAT incoherent scatter radar along the same line of sight", J. Geophys. Res. Space Physics, 121, doi:10.1002/2016JA023271, 2017

Ivchenko, N., Schlatter, N. M., Dahlgren, H., Ogawa, Y., Sato, Y., Häggström, I., "Plasma line observations from the EISCAT Svalbard Radar during the International Polar Year", Ann. Geophysicae, 35, 1143-1149, doi.org/10.5194/angeo-35-1143-2017, 2017

Kim, H., M. R. Lessard, S. L. Jones, K. A. Lynch, P. A. Fernandes, A. L. Aruliah, M. J. Engebretson, J. I. Moen, K. Oksavik, A. G. Yahnin, T. K. Yeoman, "Simultaneous Observations of Traveling Convection Vortices: Ionosphere-Thermosphere Coupling", J. geophys. Res., 122, 4943–4959, doi:10.1002/2017JA023904, 2017

Kwagala N. K., K. Oksavik, D. A. Lorentzen, M. G. Johnsen, "On the contribution of thermal excitation to the total 630.0 nm emissions in the northern cusp ionosphere", J. Geophys. Res., 122, 1, 1234-1245, doi:10.1002/2016JA023366, 2017

Lanchester, Betty, Astronomy and Geophysics, "Some remaining mysteries in the aurora", 58, 3, 3.17–3.21, doi.org/10.1093/astrogeo/atx098, 2017

Lebed', O. M., Yu. V. Fedorenko, N. F. Blagoveshchenskaya, A. V. Larchenko, V. F. Grigor'ev, S. V. Pil'gaev, "Ground-based Observations and Simulation of Ionospheric VLF Source in Experiments on Modification of the Polar Ionosphere", Geomagnetism and Aeronomy, 57, 6, 698–705, doi.org/10.1134/S0016793217060068, 2017

Mahmoudian, A., A. R. Mohebalhojeh, M. M. Farahani, W. A. Scales, M. Kosch, "Remote sensing of mesospheric dust layers using active modulation of PMWE by high-power radiowaves", J. Geophys. Res. Space Physics, 121, doi:10.1002/2016JA023388, 2017

Mottez, F., "Aurores polaires: La Terre sous le vent du Soleil", Editions Belin/Humensis, 2017

Oyama, S.-i., K. Kubota, T. Morinaga, T. T. Tsuda, J. Kurihara, M. F. Larsen, L. Cai, "Simultaneous FPI and TMA measurements of the lower thermospheric wind in the vicinity of the poleward expanding aurora after substorm onset", Journal of Geophysical Research: Space Physics, 122, 10,864–10,875, doi:10.1002/2017JA024613, 2017

Perrone L., A. V. Mikhailov, "Long-term variations of exospheric temperature inferred from foF1 observations: A comparison to ISR Ti trend estimates", J. Geophys. Res. Space Physics, 122, doi:10.1002/2017JA024193, 2017

Reidy, J. A., R. C. Fear, D. K. Whiter, B. S. Lanchester, A. J. Kavanagh, L. J. Paxton, Y. Zhang, M. Lester, "Multi-instrument observation of simultaneous polar cap auroras on open and closed magnetic field lines", J. Geophys. Res. Space Physics, 122, 4367–4386, doi:10.1002/2016JA023718, 2017

Skjæveland, Å. S., H. C. Carlson, J. I. Moen, "A statistical survey of heat input parameters into the cusp thermosphere", J. Geophys. Res. Space Physics, 122, 9622–9651, doi:10.1002/2016JA023594, 2017

Stock, W., "Estimation of Neutral Densities in the Thermosphere", Masters thesis, The Arctic University of Norway, 2017

Strelnikov, B., Szewczyk, A., Strelnikova, I., Latteck, R., Baumgarten, G., Lübken, F.-J., Rapp, M., Fasoulas, S., Löhle, S., Eberhart, M., Hoppe, U.-P., Dunker, T., Friedrich, M., Hedin, J., Khaplanov, M., Gumbel, J., and Barjatya, "Spatial and temporal variability in MLT turbulence inferred from in situ and ground-based observations during the WADIS-1 sounding rocket campaign", A. Ann. Geophysicae, 35, 547-565, doi:10.5194/angeo-35-547-2017, 2017

Taguchi, S., Y. Chiba, K. Hosokawa, Y. Ogawa, "Horizontal profile of a moving red line cusp aurora", J. Geophys. Res. Space Physics, 122, 10.1002/2016JA023115, 2017

Takahashi, T., et al., "Depletion of mesospheric sodium during extended period of pulsating aurora", J. Geophys. Res. Space Physics, 122, doi:10.1002/2016JA023472, 2017

Wang, X., C. Zhou, "Aspect dependence of Langmuir parametric instability excitation observed by EISCAT", Geophys. Res. Lett., 44, doi:10.1002/2017GL074743, 2017

Wu J., J. Wu, H. Zhao, Z. Xu, "Analysis of incoherent scatter during ionospheric heating near the fifth electron gyrofrequency", Plasma Sci. Technol., 19(4), doi:10.1088/2058-6272/aa58db, 2017

Wu, J., J. Wu, M. T. Rietveld, I. Haggstrom, Zhao, H., Z. Xu, "Altitude and intensity characteristics of parametric instability excited by an HF pump wave near the fifth electron harmonic", Plasma Sci. Technol., 19, 125303, 2017

Wu, J., J. Wu, M. T. Rietveld, I. Haggstrom, H. Zhao, Z. Xu, "The behavior of electron density and temperature during ionospheric heating near the fifth electron gyrofrequency", J. Geophys. Res. Space Physics, 122, doi:10.1002/2016JA023121, 2017

Yamazaki Y., M. Kosch, Y. Ogawa, "Average field-aligned ion velocity over the EISCAT radars", J. geophys. Res., 122, 5630–5642, doi:10.1002/2017JA023974, 2017

Publications 2018

Aikio, A. T., H. Vanhamäki, A. B. Workayehu, I. I. Virtanen, K. Kauristie, L. Juusola, S. Buchert, D. Knudsen, "Swarm Satellite and EISCAT Radar Observations of a Plasma Flow Channel in the Auroral Oval Near Magnetic Midnight", Journal of Geophysical Research: Space Physics, 23, 6, doi.org/10.1029/2018JA025409, 2018

Belova, E., M. Kawnine, I. Häggström, T. Sergienko, S. Kirkwood, A. Tjulin, "Tristatic observation of polar mesosphere winter echoes with the EISCAT VHF radar on 8 January 2014: a case study", Earth, Planets and Space, 70, 110, doi:10.1186/s40623-018-0878-5, 2018

Bjoland, L. M., "Radar studies of plasma parameters in the polar cap and the auroral zone", Ph.D. Thesis, UiT The Arctic University of Norway, 2018

Blagoveshchenskaya, N. F., T. D. Borisova, A. S. Kalishin, V. N. Kayatkin, T. K. Yeoman, I. Häggström, "Comparison of the Effects Induced by the Ordinary (O-Mode) and Extraordinary (X-Mode) Polarized Powerful HF Radio Waves in the High-Latitude Ionospheric F Region", Cosmic Research, 56, 1, 11-25, doi.org/10.1134/S0010952518010045 ISSN 0010-9525, 2018

Borisov, N., F. Honary, H. Li, "Excitation of Plasma Irregularities in the F Region of the Ionosphere by Powerful HF Radio Waves of X-Polarization", Journal of Geophysical Research: Space Physics, 123, 5246–5260, doi.org/10.1029/2018JA025530, 2018

David, T. W., D. M. Wright, S. E. Milan, S. W. H. Cowley, J. A. Davies, I. McCrea, "A study of observations of Ionospheric upwelling made by the EISCAT Svalbard Radar during the International Polar Year campaign of 2007", Journal of Geophysical Research: Space Physics, 123, DOI: 10.1002/2017JA024802, 2018

Hargreaves, J. K. , M. J. Birch, "Observations by incoherent scatter radar of related D- and F-region structuring at very high latitude", J. Atmos. Sol.-Terr. Phys., 174, 5-16, doi.org/10.1016/j.jastp.2018.01.032, 2018

James, H. G., "Propagation directions of high-frequency waves in the ionosphere", Radio Science, 53, doi.org/10.1002/2017RS006474, 2018

Jin, Yaqi, Miloch, Wojciech Jacek, Moen, Jøran Idar, Clausen, Lasse Boy Novock, "Solar cycle and seasonal variations of the GPS phase scintillation at high latitudes", Space Weather and Space Climate, 8, doi:10.1051/swsc/2018034 ISSN 2115-7251, 2018

Jin, Y., Z. Xing, Q. Zhang, Y. Wang, Y. Ma, "Polar cap patches observed by the EISCAT Svalbard Radar: A statistical study of its dependence on the solar wind and IMF conditions", J. Atmos. Sol.-Terr. Phys., doi.org/10.1016/j.jastp.2018.01.011, 2018

Jin, Y., K. Oksavik, "GPS scintillations and losses of signal lock at high latitudes during the 2015 St. Patrick's Day storm", Journal of geophysical research. Space physics, 123(9), 7943-7957, DOI: 10.1029/2018JA025933, 2018

Kwagala, N. K., "Thermally excited 630.0 nm emissions in the polar ionosphere", Ph.D. Thesis, University of Bergen, 2018

Kwagala, N. K., K. Oksavik, D. A. Lorentzen, M. G. Johnsen, K. M. Laundal,"Seasonal and Solar Cycle Variations of Thermally Excited 630.0 nm Emissions in the Polar Ionosphere", Journal of geophysical research. Space physics, 123(8), 7029-7039, DOI: 10.1029/2018JA025477, 2018

Kwagala, N. K., K. Oksavik, D. A., Lorentzen, M. G. Johnsen, "How often do thermally excited 630.0 nm emissions occur in the polar ionosphere?", Journal of Geophysical Research: Space Physics, 123, 1, 698-710, doi.org/10.1002/2017JA024744, 2018

Lee, Young-Sook, Yong Ha Kim, Kyung-Chan Kim, Young-Sil Kwak, Timothy Sergienko, Sheila Kirkwood, Magnar G. Johnsen, "EISCAT Observation of Wave-Like Fluctuations in Vertical Velocity of Polar Mesospheric Summer Echoes Associated With a Geomagnetic Disturbance", Journal of geophysical research. Space physics, 123(6), 5182-5194, DOI: 10.1029/2018JA025399, 2018

Leyser, T. B., H. G. James, B. Gustavsson, M. T. Rietveld, "Evidence of L-mode electromagnetic wave pumping of ionospheric plasma near geomagnetic zenith", Ann. Geophys., 36, 243-251, doi.org/10.5194/angeo-36-243-2018, 2018

Marchaudon, A., P.-L. Blelly, M. Grandin, A. Aikio, A. Kozlovsky, I. Virtanen, "IPIM Modeling of the Ionospheric F 2 Layer Depletion at High Latitudes During a High-Speed Stream Event", Journal of geophysical research. Space physics., 123(8), 7051-7066, DOI: 10.1029/2018JA025744, 2018

McKay, Derek, "KAIRA — The Kilpisjärvi Atmospheric Imaging Receiver Array", Doctoral Thesis, UiT The Arctic University of Norway, 2018

Rauf, A., H. Li, S. Ullah, L. Meng, B. Wang, M. Wang, "Statistical study about the influence of particle precipitation on mesosphere summer echoes in polar latitudes during July 2013", Earth, Planets and Space, 70:108, doi: 10.1186/s40623-018-0885-6, 2018

Rexer, T., B. Gustavsson, T. Leyser, M. Rietveld, T. Yeoman, T. Grydeland, "First observations of recurring HF enhanced topside ion line spectra near the fourth gyroharmonic", Journal of Geophysical Research: Space Physics, 123, 8649–8663, https://doi.org/10.1029/2018JA025822, 2018

Safargaleev, V. V., V. N. Mitrofanov, A. E. Kozlovsky, "Complex Analysis of the Polar Substorm Based on Magnetic, Optical, and Radar Observations near Spitsbergen", Geomagn. Aeron., 58:793, doi: https://doi.org/10.1134/S0016793218040151, 2018

Sergeev, V., N. Stepanov, Y. Ogawa, S. Käki, K. Kauristie, "Solar wind dependence of electric conductances and currents in the auroral zone", J. Atmos. Sol.-Terr. Phys., 177, 38-45, doi.org/10.1016/j.jastp.2017.07.006, 2018

Streltsov, A. V., J.-J. Berthelier, A. A. Chernyshov, V. L. Frolov, F. Honary, M. J. Kosch, R. P. McCoy, E. V. Mishin, M. T. Rietveld, "Past, Present and Future of Active Radio Frequency Experiments in Space", Space Science Reviews, 214:118, https://doi.org/10.1007/s11214-018-0549-7, 2018

Tereshchenko, E. D., A. D. Milichenko, M. T. Rietveld, S. M. Chernyakov, M. V. Shvets, "Change of the high-latitude ionosphere during heating by a powerful short radio wave of the EISCAT/Heating complex according to signals of the GLONASS satellite and the incoherent scattering radar", Proceedings of the Murmansk State Technical University, DOI: 10.21443/1560-9278-2018-21-1-170-181, 2018

Tsuda, T. T., M. T. Rietveld, M. J. Kosch, S. Oyama, K. Hosokawa, S. Nozawa, T. Kawabata, A. Mizuno, Y. Ogawa, "A survey of conditions for artificial aurora experiments at EISCAT Tromsø site using dynasonde data", Earth, Planets and Space, 70, 40, doi.org/10.1186/s40623-018-0805-9, 2018

Tsuda, T. T., M. T. Rietveld, M. J. Kosch, S. Oyama, Y. Ogawa, K. Hosokawa, S. Nozawa, K. Kawabata, A. Mizuno, "Survey of conditions for artificial aurora experiments by the second electron gyro-harmonic at EISCAT Tromsø using dynasonde data", Earth, Planets and Space, 70:94, doi.org/10.1186/s40623-018-0864-y, 2018

Ullah, S., H. Li, A. Rauf, L. Meng, B. Wang, M. Wang, "PMSE dependence on frequency observed simultaneously with VHF and UHF radars in the presence of precipitation", Plasma Sci. Technol., 20(11), 2018-11-115302, 2018

Virtanen, I., B. Gustavsson, A. Aikio, A. Kero, K. Asamura, Y. Ogawa, "Electron Energy Spectrum and Auroral Power Estimation From Incoherent Scatter Radar Measurements", Journal of geophysical research. Space physics, 123(8), 865-6887, DOI: 10.1029/2018JA025636, 2018

Wang, X., C. Zhou, M. Liu, F. Honary, B. Ni, Z. Zhao, "Threshold of parametric instability in the ionospheric heating experiments", Plasma Sci. Technol., 20(11), 2018-11-115301, 2018

Wang, X., C. Zhou, Adv. Space Res., "Electron density inversed by plasma lines induced by suprathermal electron in the ionospheric modification experiment", 61, 2252-2258, doi: 10.1016/j.asr.2018.02.001, 2018

Wu, J., J. Wu, M. T. Rietveld, I. Haggstrom, Z. Xu, H. Zhao, "The extending of observing altitudes of plasma and ion lines during ionospheric heating", Journal of Geophysical Research: Space Physics, 123, doi.org/10.1002/2017JA024809, 2018

Wu, J., J. Wu, M. T. Rietveld, I. Haggstrom, H. Zhao, T. Xu, Z. Xu, "Systematic variation in observing altitude of enhanced ion line by the pump near fifth gyroharmonic", Plasma Science and Technology, 20, 12, doi:10.1088/2058-6272/aadd44, 2018

Yamauchi, M., T. Sergienko, C.-F. Enell, A. Schillings, R. Slapak, M. G. Johnsen, A. Tjulin, H. Nilsson, "Ionospheric response observed by EISCAT during the September 6-8 2017 space weather event: overview", Space weather : the international journal of research & applications, 16(9), 1437-1450, DOI: 10.1029/2018SW001937, 2018

Yang, J., Q. Li, J. Wang, S. Hao, G. Ma, "The polarization characteristics of ELF/VLF waves generated via HF heating experiments of the ionosphere by EISCAT", Physics of Plasmas, 25, 092902, doi: 10.1063/1.5044611, 2018

EISCAT Operations 2017 and 2018

The EISCAT radars operate in two basic modes, using approximately half the available observing time for each. In the Special Programme mode, users conduct individual experiments dedicated to specific experiments and objectives. The resulting data are reserved for the exclusive use of the experimenters for one year from the date of collection. Special programmes often make use of the well developed pulse schemes and observing modes of the Common Programme. EISCAT Common Programmes are conducted for the benefit of the entire user community and the resulting data are immediately available to all.

The UHF and VHF radars are often operated simultaneously during the Common Programme experiments. Such observations offer comprehensive data sets for atmospheric, ionospheric, and magnetospheric studies.

Common Programme One, CP-1, uses a fixed transmitting antenna, pointing along the geomagnetic field direction. The three-dimensional velocity and anisotropy in other parameters are measured by means of the VHF receiving stations at Kiruna and Sodankylä. CP-1 is capable of providing results with very good time resolution and is suitable for the study of substorm phenomena, particularly auroral processes where conditions might change rapidly. Continuous electric field measurements are derived from the tri-static F-region data. On longer time scales, CP-1 measurements support studies of diurnal changes, such as atmospheric tides, as well as seasonal and solar-cycle variations.

Common Programme Two, CP-2, is designed to make measurements from a small, rapid transmitter antenna scan. One aim is to identify wave-like phenomena with length and time scales comparable with, or larger than, the scan (a few tens of kilometers and about ten minutes). The first three positions form a triangle with vertical, south, and south-east positions, while the fourth is aligned with the geomagnetic field.

Common Programme Three, CP-3, covers a 10° latitudinal range in the F-region with a 17-position scan up to 74°N in a 30 min cycle. The observations are made in a plane defined by the magnetic meridian through Tromsø. The principal aim of CP-3 is the mapping of ionospheric and electrodynamic parameters over a broad latitude range.

Common Programme Four, CP-4, covers geographic latitudes up to almost 80°N (77°N invariant latitude) using a low elevation, split-beam configuration. CP-4 is particularly suitable for studies of high latitude plasma convection and polar cap phenomena. However, with the present one-beam configuration of the VHF radar, CP-4 is run with either both UHF and VHF radars or with UHF only in a two position scan.

Common Programme Six, CP-6, is designed for low altitude studies, providing spectral measurements at mesospheric heights. Velocity and electron density are derived from the measurements and the spectra contain information on the aeronomy of the mesosphere. Vertical antenna pointing is used.

Common Programme Seven, CP-7, probes high altitudes and is particularly aimed at polar wind studies. The present version, with only one of the VHF klystrons running, is designed to cover altitudes up to 1500 km vertically above Ramfjordmoen.

Equivalent Common Programme modes are available for the EISCAT Svalbard Radar: CP-1 is directed along the geomagnetic field (81.6° inclination). CP-2 uses a four position scan. CP-3 is a 15 position elevation scan with southerly beam swinging positions. CP-4 combines observations in the F-region viewing area with field-aligned and vertical measurements. CP-6 is similar to the mainland radar CP-6. CP-7 is similar to the mainland radar CP-7.

The tables on the next four pages summarise the accounted hours on the various facilities for each month and for each Common Programme mode (CP) or Associate (SP) for the years 2017 and 2018.

KST COMMON PROGRAMMES

2017	Jan	Feb	Mar	Apr	May	Jun	Jul	Aug	Sept	Oct	Nov	Dec	Total	%	Target%
CP1													0	0	16
CP2	202.5	56											258.5	33	16
CP3													0	0	12
CP4	194								136.5			145.5	476	60	10
CP6						56.5							56.5	7	20
CP7													0	0	18
UP													0	0	
Total	396.5	56	0	0	0	56.5	0	0	136.5	0	0	145.5	**791**	100	
%	50	7	0	0	0	7	0	0	17	0	0	18	100		

KST SPECIAL PROGRAMMES

2017	Jan	Feb	Mar	Apr	May	Jun	Jul	Aug	Sept	Oct	Nov	Dec	Total	Incl AA	Move	Target
CN											80		80	92		104
FI				3	15		12.5				80		110.5	123		108
NI	14.5	15.5	64.5					11.5				16	122	135	23	137
NO	5	2.5	36.5				12.5	20		36.5	3	22	138	162	-16	192
SW	11	27.5	29					37		13		8	125.5	149		208
UK	11.5	10.5	6.5				12.5					7	48	60		103
AA	3					12	20	21	20	20			96			
Total	45	56	136.5	3	15	12	57.5	89.5	20	69.5	163	53	**720**	**720**	**7**	**844**
%	6	8	19	0	2	2	8	12	3	10	23	7	100			

	EI	CN	FI	NI	NO	SW	UK	
Target		12.3	12.77	13.52	24.61	24.61	12.18	%

KST OTHER PROGRAMMES

2017	Jan	Feb	Mar	Apr	May	Jun	Jul	Aug	Sept	Oct	Nov	Dec	Total	Target
PP		10	16	3	15			3			9.5	7.5	64	70
EI							12.5	0.5					13	33
RU													0	0
FR			10										10	6
UA													0	5
KR													0	0
TB										7.5			7.5	8
Total	0	10	26	3	15	0	12.5	3.5	0	7.5	9.5	7.5	**94.5**	**199**

KST TOTALS

2017	Jan	Feb	Mar	Apr	May	Jun	Jul	Aug	Sept	Oct	Nov	Dec	Total	Target
CP	396.5	56	0	0	0	56.5	0	0	136.5	0	0	145.5	791	708
SP	45	56	136.5	3	15	12	57.5	89.5	20	69.5	163	53	720	837
OP	0	10	26	3	15	0	12.5	3.5	0	7.5	9.5	7.5	94.5	199
Total	441.5	122	162.5	6	30	68.5	70	93	156.5	77	172.5	206	**1605.5**	**1743**

USAGE BREAKDOWN

2017	Jan	Feb	Mar	Apr	May	Jun	Jul	Aug	Sept	Oct	Nov	Dec	Total	Target
UHF	239.5	100.5	118.5	4	20	13.5	20	31	28.5	50.5	53.5	47	726.5	658
VHF	146	1.5	24	2	10	40	24	47	95	2	50	116	557.5	733
ESR	354	90.5	30.5	0	0	38	0	8	93	0	92	158.5	864.5	877
Heating		19	20.5				16	5.5		23	62		146	232
Total Radar	739.5	211.5	173	6	30	91.5	44	86	216.5	52.5	195.5	321.5	2148.5	2500
Low Power V													0	
Passive KST	290	3				78	46	50	166	4	36	215.5	888.5	600
Passive ESR													0	

ESR COMMON PROGRAMMES

2017	Jan	Feb	Mar	Apr	May	Jun	Jul	Aug	Sept	Oct	Nov	Dec	Total	%	Target%
CP1	36	5							16		0.5		57.5	10	54
CP2	127.5	50									1		178.5	32	16
CP3													0	0	12
CP4	139		0.5						72.5		0.5	75.5	288	51	10
CP6						38			2.5				40.5	7	
CP7													0	0	
UP													0	0	
Total	302.5	55	0.5	0	0	38	0	0	91	0	2	75.5	**564.5**	100	
%	54	10	0	0	0	7	0	0	16	0	0	13	100		

ESR SPECIAL PROGRAMMES

2017	Jan	Feb	Mar	Apr	May	Jun	Jul	Aug	Sept	Oct	Nov	Dec	Total	Incl AA	Move	Target
CN											15		15	15		51
FI											27	24	51	51		53
NI	16		6									12	34	34	-23	33
NO		18.5	24					8	2		48	15	115.5	116	16	118
SW	12.5	12										19.5	44	44		102
UK	23	5										4.5	32.5	33		50
AA													0			
Total	51.5	35.5	30	0	0	0	0	8	2	0	90	75	**292**	**292**	**-7**	**413**
%	18	12	10	0	0	0	0	3	1	0	31	26	100			

ESR OTHER PROGRAMMES

2017	Jan	Feb	Mar	Apr	May	Jun	Jul	Aug	Sept	Oct	Nov	Dec	Total	Target
PP												8	8	0
EI													0	18
RU													0	0
FR													0	0
UA													0	0
KR													0	34
TB													0	3
Total	0	0	0	0	0	0	0	0	0	0	0	8	**8**	**72**

ESR TOTALS

2017	Jan	Feb	Mar	Apr	May	Jun	Jul	Aug	Sept	Oct	Nov	Dec	Total	Target
CP	302.5	55	0.5	0	0	38	0	0	91	0	2	75.5	564.5	315
SP	51.5	35.5	30	0	0	0	0	8	2	0	90	75	292	420
OP	0	0	0	0	0	0	0	0	0	0	0	8	8	72
Total	354	90.5	30.5	0	0	38	0	8	93	0	92	158.5	**864.5**	**877**

KST COMMON PROGRAMMES

2018	Jan	Feb	Mar	Apr	May	Jun	Jul	Aug	Sept	Oct	Nov	Dec	Total	%	Target%
CP1	63	0.5			1	63		0.5					128	23	16
CP2	198												198	35	16
CP3									119.5				119.5	21	12
CP4		121.5											121.5	21	10
CP6													0	0	20
CP7													0	0	18
UP													0	0	
Total	261	122	0	0	1	63	0	0.5	119.5	0	0	0	**567**	100	
%	46	22	0	0	0	11	0	0	21	0	0	0	100		

KST SPECIAL PROGRAMMES

2018	Jan	Feb	Mar	Apr	May	Jun	Jul	Aug	Sept	Oct	Nov	Dec	Total	Incl AA	Move	Target
CN											31.5	27	58.5	68		93
FI											92.5		92.5	103		97
NI		50	12						4		11	32	109	120	8	111
NO	12		20.5	16.5				47		29.5			125.5	145	-20	167
SW	16			14.5				41					71.5	91		187
UK	12	7.5	35.5	10			7			14		6	92	102		92
AA									20	24	20	16	80			
Total	40	57.5	68	41	0	0	7	88	24	67.5	155	81	**629**	**629**	**-12**	**759**
%	6	9	11	7	0	0	1	14	4	11	25	13	100			

	EI	CN	FI	NI	NO	SW	UK	
Target		12.3	12.77	13.52	24.61	24.61	12.18	%

KST OTHER PROGRAMMES

2018	Jan	Feb	Mar	Apr	May	Jun	Jul	Aug	Sept	Oct	Nov	Dec	Total	Target
PP			24.5	32.5		12							69	81
EI										4			4	33
RU										12			12	0
FR													0	6
UA													0	5
KR						16.5							16.5	0
TB					7.5								7.5	8
Total	0	0	24.5	32.5	7.5	28.5	0	0	0	16	0	0	**109**	**210**

KST TOTALS

2018	Jan	Feb	Mar	Apr	May	Jun	Jul	Aug	Sept	Oct	Nov	Dec	Total	Target
CP	261	122	0	0	1	63	0	0.5	119.5	0	0	0	567	540
SP	40	57.5	68	41	0	0	7	88	24	67.5	155	81	629	771
OP	0	0	24.5	32.5	7.5	28.5	0	0	0	16	0	0	109	210
Total	301	179.5	92.5	73.5	8.5	91.5	7	88.5	143.5	83.5	155	81	**1305**	**1521**

USAGE BREAKDOWN

2018	Jan	Feb	Mar	Apr	May	Jun	Jul	Aug	Sept	Oct	Nov	Dec	Total	Target
UHF	293	43.5	84.5	25	11.5	91.5	6	11.5	139.5	56	100.5	17	879.5	602
VHF	8	100.5	8	34.5				47.5					198.5	602
ESR	384.5	117	37.5	0	0	45	0	0.5	86.5	1	81	144	897	1068
Heating				14			1	11.5		23.5	21	26	97	197
Total Radar	685.5	261	130	59.5	11.5	136.5	6	59.5	226	57	181.5	161	1975	2469
Low Power V													0	
Passive KST		175						86.5				40	301.5	600
Passive ESR													0	

ESR COMMON PROGRAMMES

2018	Jan	Feb	Mar	Apr	May	Jun	Jul	Aug	Sept	Oct	Nov	Dec	Total	%	Target%
CP1	75					45		0.5	48.5				169	35	54
CP2	188												188	39	16
CP3									38				38	8	12
CP4		87											87	18	10
CP6													0	0	
CP7													0	0	
UP													0	0	
Total	263	87	0	0	0	45	0	0.5	86.5	0	0	0	**482**	100	
%	55	18	0	0	0	9	0	0	18	0	0	0	100		

ESR SPECIAL PROGRAMMES

2018	Jan	Feb	Mar	Apr	May	Jun	Jul	Aug	Sept	Oct	Nov	Dec	Total	Incl AA	Move	Target
CN											20	22	42	42	0	53
FI											44	9	53	53	0	55
NI		13	12									28.5	53.5	54	-8	50
NO	12	11.5								1	17	29.5	71	71	20	126
SW	33											22.5	55.5	56	0	106
UK	26.5	5.5	25.5									24.5	82	82	0	53
AA													0			
Total	71.5	30	37.5	0	0	0	0	0	0	1	81	136	**357**	**357**	**12**	**432**
%	20	8	11	0	0	0	0	0	0	0	23	38	100			

ESR OTHER PROGRAMMES

2018	Jan	Feb	Mar	Apr	May	Jun	Jul	Aug	Sept	Oct	Nov	Dec	Total	Target
PP	10											8	18	46
EI													0	17
RU													0	0
FR													0	0
UA													0	0
KR	40												40	34
TB													0	0
Total	50	0	0	0	0	0	0	0	0	0	0	8	**58**	**97**

ESR TOTALS

2018	Jan	Feb	Mar	Apr	May	Jun	Jul	Aug	Sept	Oct	Nov	Dec	Total	Target
CP	263	87	0	0	0	45	0	0.5	86.5	0	0	0	482	315
SP	71.5	30	37.5	0	0	0	0	0	0	1	81	136	357	420
OP	50	0	0	0	0	0	0	0	0	0	0	8	58	97
Total	384.5	117	37.5	0	0	45	0	0.5	86.5	1	81	144	**897**	**1068**

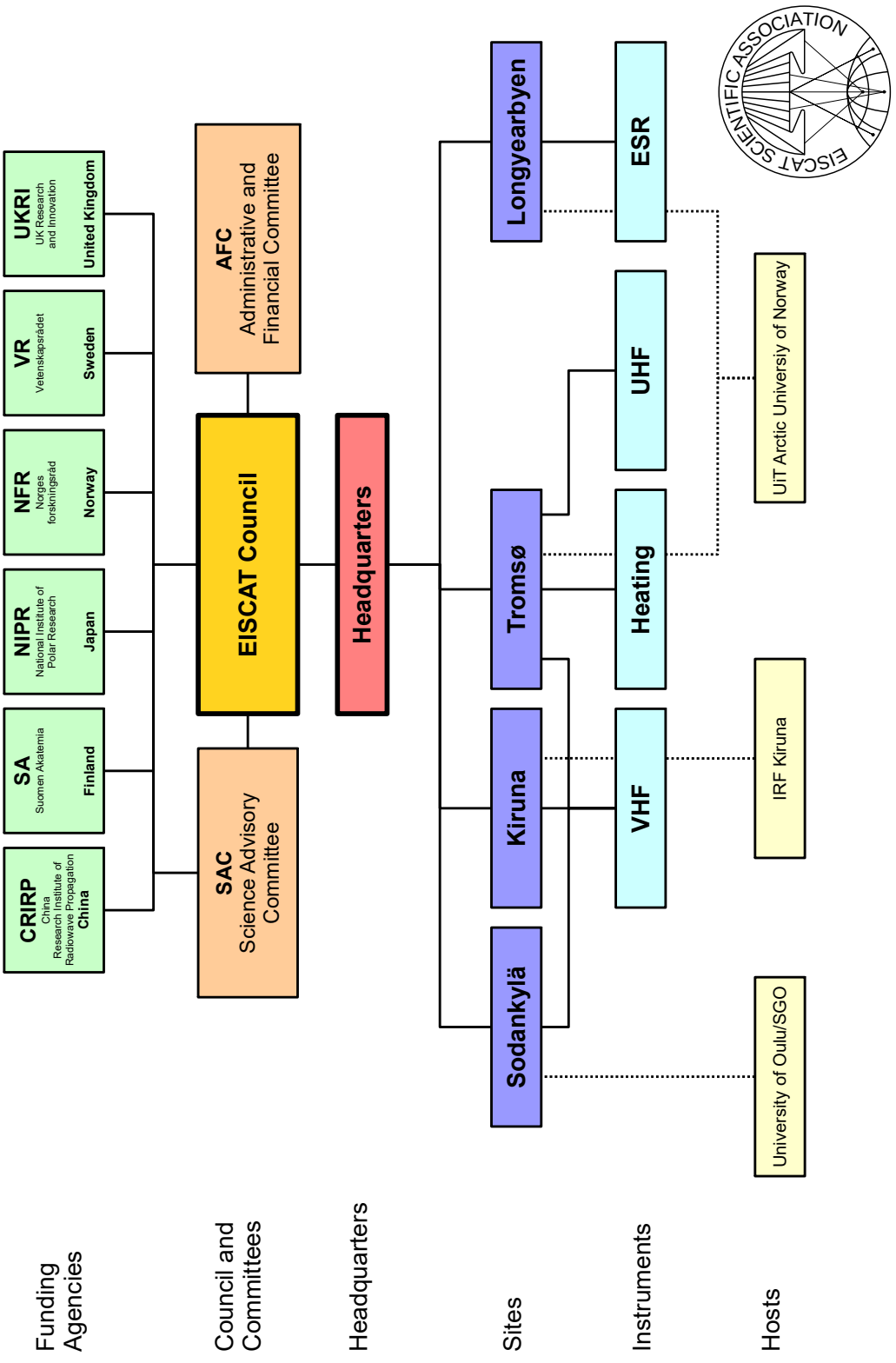

EISCAT organisational diagram, December 2018.

Photo from the Annual Review Meeting, 25–28 September 2018, at Lofoten Arctic Hotel Skata, Hennings-vær,Norway. From left: Johan Svensson, Craig Heinselman, Assar Westman, Carl-Fredrik Enell, Guttorm Mikalsen, Emma Unander, Mike Rietveld, Martin Langteigen, Elisabet Goth, Hans-Erik Fjeld, Anders Tjulin, Erlend Danielsen, Peter Bergqvist, Robert Juhlin, Rikard Slapak, Harri Hellgren, Simon Brown, Arild Stenberg, Espen Helgesen.

EISCAT Scientific Association

December 2018

Council

The Council consists of a Delegation with a maximum of three persons from each Associate.

Finland	
Prof. A. Aikio	
Dr. K. Sulonen	Delegate
Japan	
Prof. H. Miyaoka	*Chair*, Delegate
Dr. S. Nozawa	
Norway	
Prof. I. Mann	*Vice-Chair*
Prof. K. Ruud	Delegate
P. R. of China	
Dr. Z. Ding	
Prof. J. Wu	Delegate
Sweden	
Dr. T. Andersson	Delegate
Prof. J. Gumbel	
United Kingdom	
Prof. M. Freeman	Delegate
Dr. I. McCrea	

Scientific Advisory Committee

The EISCAT scientific community organises the Scientific Oversight Committee (SAC), under the guidance of the Council.

Prof. L. Baddeley	Norway
Dr. S. Buchert	*Chairperson*, Sweden
Dr. K. Chau	External member
Dr. G. Jee	S. Korea (affiliated)
Dr. A. Kavanagh	United Kingdom
Dr. Y.-S. Kwak	S. Korea (affiliated)
Dr. Y. Ogawa	Japan
Dr. F. Pitout	France (affiliated)
Dr. T. Ulich	Finland
Dr. J. Wu	P. R. of China
Dr. A. Zalizovsky	Ukraine

Director

Dr. C. Heinselman

Administrative and Finance Committee

The Administrative and Finance Committee (AFC) advises the EISCAT Council on matters relating to administrative, financial and legal issues.

Mr. H. Andersson	Head of Administration
Mr. B. Clark	United Kingdom
Dr. M. Friberg	*Chairperson*, Sweden
Dr, C. Heinselman	Director
Dr. I. Solheim	Norway
Mr. M. Suehiro	Japan
Ms. M. Vannas	Finland
Dr. B. Xu	P. R. of China

Executives

Senior Management

Mr. H. Andersson	Head of Adm., Deputy Dir.
Dr. C. Heinselman	Director

Site Leaders

Station Managers

Mr. E. Helgesen	EISCAT Svalbard Radar
Mr. L. Lövqvist	Kiruna Site
Mr. J. Markkanen	Sodankylä Site
Dr. M. Rietveld	Tromsø Radar & Heating

Appendix:

EISCAT Scientific Association Annual Report, 2017

EISCAT Scientific Association
Registered as a Swedish non-profit organisation
Organisation number: 897300-2549

Annual financial report for the year 2017-01-01 – 2017-12-31

The EISCAT Council and the Director for the Association submits herewith the annual report for 2017.

Content	**Page**
Administration report	1
Profit and loss accounts	5
Balance sheet	6
Statement of cash flows	7
Notes	8

ADMINISTRATION REPORT

Ownership, organisation and objective

The EISCAT Scientific Association was established in 1975 through an agreement between six European organisations. Japan joined in 1996 and the Peoples Republic of China in 2007.

The EISCAT Associates at 2017-12-31 are: China Research Institute of Radiowave Propagation (Peoples Republic of China), National Institute of Polar Research (Japan), Natural Environment Research Council (United Kingdom of Great Britain and Northern Ireland), Norges forskningsråd (Norway), Suomen Akatemia (Finland), and Vetenskapsrådet (Sweden).

The now running EISCAT Agreement came into force 2017-06-20, with all Associates making long term funding commitments to the Association. The Association has its formal seat in Kiruna, Sweden, and is registered as a non-profit organisation.

The aim of the Association is to make significant progress in the understanding of physical processes in geospace, in the high latitude atmosphere, and in the coupling between the high and low latitudes and altitudes. For this purpose, the Association has developed, constructed, and now operates, a number of radar facilities at high latitudes. At present, these comprise a system of stations at Tromsö (Norway), Kiruna (Sweden), Sodankylä (Finland), and Longyearbyen (Svalbard).

The Association is fully funded by the Associates, but additional operations may also be funded by short term additional contributions from both Associate and non-Associate bodies. Depending on the available funding, scientific priorities and operational targets are adjusted on an annual basis.

The EISCAT Council is charged with the overall administration and supervision of the Association's activities. The Council appoints a Director, who is responsible for the daily management and operation of the facilities of the Association.

Operation and scientific development

The EISCAT Radars delivered a full programme of operations for the user community and operated reliably throughout the year.

The various EISCAT radars operated for a total of 2 480 accounted hours (2 726 hours in 2016).

Common Programmes amounted to 54% (53%) of the operations. Special Programmes amounted to 41% (39%) and other operations amounted to 5% (8%) of the total hours.

IRAP-CNRS (France), KASI (South Korea), KOPRI (South Korea) and IRA-NASU (Ukraine) have Affiliate agreements and totally 10 hours (90 hours) were affiliates accounted. The Peer-Review Programme made it possible for user groups from Japan, Germany and USA to run experiments, at no cost, on the systems. Peer-Review time amounted to 82 accounted hours (85 hours).

Future operation and scientific development
All systems are ready for users. These comprise now of the EISCAT Svalbard Radar, Heating and the UHF and VHF radars with the possibility to run the VHF in tristatic mode by using the antennas in Kiruna and Sodankylä for reception.

In September, the build project of the new EISCAT_3D system started. The EISCAT_3D system will replace the current UHF and VHF radar systems. The new system comprises of three phased arrays working together. These will be built in Finland, Norway and Sweden. Construction works of the Norwegian EISCAT_3D site, located near Skibotn, Storfjord kommune, Norway, will start already summer 2018.

The new EISCAT_3D system will be ready for users towards the end of 2021.

Project activities
Three projects ended during the year, the European Commission funded EGI-Engage and EISCAT3D_PfP projects and the Vetenskapsrådet, Sweden, funded VR-OG project.

Two new European Commission funded projects were agreed during the year. One, AARC2 "Authentication and Authorisation For Research and Collaboration" started 2017-05-01 and the second, EOSC-Hub "Integrating and managing services for the European Open Science Cloud" starts 2018-01-01. Both are under the H2020-EINFRA topic.

EISCAT is currently also participating in the COOP_Plus and ENVRI_Plus EC-funded projects.

The EISCAT3D_PfP project successfully ended 2017-08-31. The project schedule was well kept though some of the delivered parts did not function as hoped. The project was financially reviewed by an external auditor and a Brussels held final review took place on 2017-10-09. The final review concluded that the "Project has achieved most of its objectives and milestones for the period with relatively minor deviations".

In the spring EISCAT Council meeting, the go-ahead decision to start the EISCAT_3D implementation project was made. The first phase, Stage 1, has a budget volume of about 685 MSEK and will run for about four years. The project was officially started at a kick-off event held in Tromsø and Skibotn, Norway, 2017-09-07. About 75 persons attended the kick-off.

The work of the Council and its committees
The Council had two ordinary meetings, and a follow-on telecon, during the year. On 2017-04-24, Council agreed that the funding agencies and Council is in a position to decide to start the implementation of EISCAT_3D at its next regular meeting, in Tokyo. The first regular meeting was held 2017-05-31 -06-01, in Tokyo, Japan, and the second meeting was held 2017-11-13 -14, in Oulu, Finland. The meetings were chaired by Prof. Hiroshi Miyaoka.

In the Tokyo meeting, Council decided to start the EISCAT_3D implementation project by activating the first phase of the project, Stage 1.

EISCAT_3D Stage 1 (project acronym E3DS1) comprises of the EISCAT_3D core transmit/receive array plus outriggers in or near Skibotn, Norway, and EISCAT_3D receive arrays in or near Karesuvanto, Finland and Kaiseniemi, Sweden.

In June, the new EISCAT agreement came into force.

With the new agreement, two new committees were introduced, Scientific Advisory Committee (SAC) and the Administrative and Finance Committee (AFC). SAC is instead of the previous Scientific Oversight Committee and AFC formalises the already going AdHoc established administration and finance committee.

Both SOC/SAC and AFC had two meetings each during the year.

In the Oulu meeting, Council agreed to extend the employment contract with the present Director, Dr. Craig Heinselman for another three-year period following onto his current contract that ends at the end of 2018.

Budget development during the year
The 2017 operations ended slightly below the operating target set for the year.

The overall spend followed well the prediction for the year and the regular income was close to forecasted. Income from project work was more than budgeted.

In total, the year ended in a net profit.

The long-term budget plan
The long-term budget plan is challenging. The introduction of EISCAT_3D will have operation cost implications due to the higher transmitter output, several-thousand receiver channels and powerful computer clusters. Most Associates have though agreed to substantially increase their annual contributions to cover the additional operating costs. Nevertheless, the challenge lies in to keep the current systems operational, build the new, and later phase out, and decommission, the old systems, while maintaining a reasonable operating hours level throughout the process.

The result for 2017 and profit/loss handling
The year ended in a net profit of 3 627 kSEK and it is planned to put the amount in the designated funds reserve for use in subsequent years.

PROFIT AND LOSS ACCOUNTS

in thousands of Swedish Crowns

	Note 1	*2017*	*2016*
Income from operations			
Grants received	Note 2	46 774	38 985
Revenue from operations	Note 3	89	219
Other income from operations	Note 4	306	294
		47 169	39 498
Expenses from operations			
Operation costs	Note 5	-14 557	-10 276
Administration costs		-4 581	-4 033
Personnel costs	Note 6	-21 884	-21 375
Depreciation of fixed assets		-2 174	-1 983
		-43 197	-37 667
Operating profit/loss		**3 972**	**1 831**
Financial items			
Interest income		12	6
Other financial income and cost		263	1 004
		275	1 009
Net profit/loss for the year		**4 247**	**2 840**

Changes in designated funds	Note 7		
Net profit/loss for the year		4 247	2 840
Use of designated funds from previous years		511	777
Allocation of designated funds received during the year, but not used		-1 130	-4 408
Net profit/loss for the year after redistributions		**3 627**	**-791**

BALANCE SHEET

in thousands of Swedish Crowns

		2017	*2016*
ASSETS			
Fixed assets			
Tangible fixed assets	Note 8		
Buildings		1 808	2 033
Radar systems		4 279	4 549
Equipment and tools		2 831	2 837
		8 918	9 419
Current assets			
Receivables		24 519	2 385
Prepayments and accrued income	Note 9	2 258	8 530
Cash at bank and in hand	Note 10	76 109	36 318
		102 885	47 233
Total assets		**111 804**	**56 652**
CAPITAL AND LIABILITIES			
Capital			
Funds invested	Note 11	8 918	9 419
Designated funds	Note 12	20 978	20 650
Net income for the year after redistribution		3 627	-791
		33 524	29 277
Current liabilities			
Accounts payable, trade		5 020	5 830
EISCAT_3D build grants received but not used	Note 13	55 435	0
External project grants received but not used	Note 14	17 445	21 115
Other liabilities		379	429
		78 280	27 374
Total capital and liabilities		**111 804**	**56 652**

STATEMENT OF CASH FLOWS

in thousands of Swedish Crowns

	2017	*2016*
Operating activities		
Operating result before financial items	3 972	1 831
Transfer from funds invested	2 174	1 983
Interest received	12	6
Currency exchange rate changes	263	1 004
Extra ordinary income and cost	0	0
Increase/decrease of receivables	-22 134	-786
Increase/decrease of prepayments and accrued income	6 273	-6 025
Increase/decrease of creditors and liabilities	50 905	2 471
Cash flow from operations	**41 465**	**482**
Investment activities		
Investments in tangible assets	-1 674	-1 206
Cash flow from investment activities	**-1 674**	**-1 206**
Cash flow for the year	**39 791**	**-723**
Liquid assets at the beginning of the year	**36 318**	**37 041**
Liquid assets at the end of the year	**76 109**	**36 318**

NOTES	2017	2016

Note 1 *Accounting principles*

The accounting and valuation principles applied are consistent with the provisions of the Swedish Annual Accounts Act and generally accepted accounting principles (for 2017 onwards, bokföringsnämnden allmänna råd och vägledningar, BFNAR 2012:1 K3).

All amounts are in thousands of Swedish kronor (SEK) unless otherwise stated.

Income

Received grants are reported as income in the period when they were claimed or received. Conditional grants are recognised as income when the associated conditions have been met. Income and revenue from operations, which include own-account funds, are reported as income when they were claimed or received. Grants and other income in foreign currencies have been accounted in the amounts estimated to be received, based on individual assessment.

Employee benefits

Ongoing remuneration to employees, either direct employed or provided via host agreements, in the form of salaries, social security, contributions to pension schemes and staff related insurances are accounted as personnel costs. Other remunerations, in cash, like travel subsistences or as benefits in-kind, like clothing, training and health care are also accounted as personnel costs. Overhead cost on host provided personnel is considered as external services accounted as administration cost.

Financial income

Dividends and interest income are accounted when credited the account.

Receivables

Receivables are stated at the amounts estimated to be received, based on individual assessment.

Receivables and payables in foreign currencies

Receivables and payables in foreign currencies are valued at the closing day rate. Where hedging measures have been used, such as forwarding contracts, the agreed exchange rate is applied. Gains and losses relating to operations are accounted for under other financial income and cost.

Bank accounts in foreign currencies

Bank balances in foreign currencies are valued at the closing day rate.

Fixed assets

Tangible fixed assets are stated at their original acquisition values after deduction of depreciation according to plan. Assets are depreciated systematically over their estimated useful lives. The following periods of depreciation are applied: Buildings 5 - 50 years, Radar systems 3 - 30 years and Equipment and tools 1 - 5 years.

Note 2 Grants received

The Associates contributed to the operation during the year in accordance with the EISCAT agreement. The Affiliates contributed according to agreed annual commitments. Income from European Commission (EC) funded projects were also accounted as received grants. The E3DS1 project started 2017-09-01 and the resulting projects costs were covered jointly by VR (Sweden) and NERC (UK). The VR funded project towards EISCAT_3D realisation continued throughout the year. It ended 2017-12-31. All projects were funded via prefinancing where costs were covered by transfers from pre-received funds.

	2017	2016
Associates	22 522	22 248
Affiliates	796	1 399
Project grants, EC	19 458	14 040
Project grant, E3DS1	1 625	0
Project grant, VR-OG	2 374	1 297
	46 774	38 985

Accumulated Associate contributions status as of 2017-12-31

Annual contributions included and for 2017, NERC, NIPR and VR were credited for providing EISCAT_3D and E3DS1 project related funds. These sums are used for EISCAT's ownership and time-share calculation

Previous Associates	382 168	382 168
CRIRP (P. R. of China)	37 245	33 413
NIPR (Japan)	80 057	78 189
RCN (Norway)	178 203	172 861
SA (Finland)	85 559	81 980
NERC (United Kingdom)	238 187	234 228
VR (Sweden)	163 597	153 907
	1 165 016	1 136 747

Note 3 Revenue from operations

The Association can, at rates related to the costs involved and as available, sell observation hours to Associates, Affiliates and other parties. Income from such selling of time are considered to be revenue. In 2017, 7,5 hours were provided to so called time-buyers.

Income from time-buyers	89	219

Note 4 Other income from operations

The Association supports visiting users by offering site accommodation and equipment hosting for either campaign brought instruments or deployed for longer periods. Educational support is done by providing teachers and/or other resources (like laboratory support). Associates and/or user-groups contribute occasionally to system improvements by funding, of own interest, certain repairs or hardware changes.

Accommodation	143	124
Instrument hosting agreements	21	21
Educational support	18	48
Other income	123	101
	306	294

Note 5 *Operations*

The annual operating target for all systems together is usually about 2 500 active (high power mode) hours. For 2017, the budget assumed 2 467 hours and the outcome became 2 295 hours. Passive hours come in addition. Such hours have a minimal effect on cost since the systems do not draw more electricity than in an off mode. The accounted hours are usually lower than the operating hours total since some systems have a charge rate that is less than 1-to-1.

Active (high-power)	*Hours*	*Hours*
EISCAT Svalbard Radar	865	974
UHF system	727	844
VHF system	558	609
Heating system	146	123
	2 295	2 549
Passive (receive only)		
Kiruna receiver system	444	444
Sodankylä receiver system	444	444
	889	889

	2017	2016

Note 6 *Personnel costs and average number of employees*

The Association employs directly Headquarters and most project staff, currently about ten positions, including the Director. Of these, three are on shorter-term project employments. The Headquarters is located in Kiruna, Sweden. The personnel working at the Kiruna (Sweden), Sodankylä (Finland), Svalbard and Tromsö (Norway) sites are normally not employed by the Association. Instead, the personnel are provided via site contracts by the Swedish Institute of Space Physics (Kiruna site staff), Oulu University (Sodankylä staff) and the Arctic University of Norway (Tromsö and Svalbard staff). The Association refunds all expenses related to the provided staff, as well as an additional overhead.

Personnel costs in total		
Salaries and emoluments paid to the Director	1 920	1 831
Other personnel, employed and provided via site contracts	13 322	13 078
Social security contributions amounted to	6 274	5 920
of which for pension costs	*3 061*	*2 986*
Other personnel costs	369	545

The Director, Dr. Craig Heinselman, started his employment 2013-01-01. His current employment contract ends 2018-12-31.

Of the pension costs, 306 kSEK (295 kSEK) relates to the Director. He and all other directly employed staff are included in ITP like occupational pension plans. For the personnel provided via site contracts, the pension plans are handled by their respective employer.

The members of the board (EISCAT Council) and members of committees, who represents Associates and Affiliates, do not receive remunerations from the Association. Travel expenses in connection with Council and committee meetings are normally covered by the Associates and Affiliates. The Association reimburses though the travel costs for Committee Chairpersons and external members.

Salaries and emoluments and average number of staff per country

Finland		
Salaries and emoluments	453	655
Average number of staff - men and women	1 + 0	1 + 0
Norway (including Svalbard)		
Salaries and emoluments	5 314	5 924
Average number of staff - men and women	9 + 0	10 + 0
Sweden		
Salaries and emoluments	9 475	8 331
Average number of staff - men and women	10 + 2	10 + 2

Members of the board and Directors at year-end - men and women

The board consist of delegations from every Associate country each having a Delegate (formal member) and up to two Representatives.

Board members (EISCAT Council)	9 + 4	12 + 3
Directors	1 + 0	1 + 0

	2017	2016

Note 7 *Changes in designated funds*

Positive numbers - use of designated funds from previous years. Negative - transfer to the reserve or fund for later use.

Net profit/loss for the year	4 247	2 840
Changes to spare parts reserve	6	-3
Changes to capital operating reserve	4	-535
Changes to surplus fund	-1 130	-3 870
Changes to funds invested	500	777
	3 627	-791

Note 8 *Tangible fixed assets*

Changes in tangible fixed assets.

Buildings		
Opening acquisition value	42 471	42 471
Acquisitions during the year	6	0
Disposals during the year	0	0
Closing acquisition value	42 478	42 471
Opening accumulated depreciation	-40 439	-40 207
Depreciations during the year	-231	-232
Disposals during the year	0	0
Closing accumulated depreciation	-40 670	-40 439
Closing residual value	1 808	2 033
Radar systems		
Opening acquisition value	250 259	250 087
Acquisitions during the year	501	172
Disposals during the year	0	0
Closing acquisition value	250 760	250 259
Opening accumulated depreciation	-245 709	-245 002
Depreciations during the year	-771	-707
Disposals during the year	0	0
Closing accumulated depreciation	-246 480	-245 709
Closing residual value	4 279	4 549
Equipment and tools		
Opening acquisition value	33 844	32 902
Acquisitions during the year	1 166	1 034
Disposals during the year	19	92
Closing acquisition value	34 992	33 844
Opening accumulated depreciation	-31 008	-30 055
Depreciations during the year	-1 172	-1 044
Disposals during the year	19	92
Closing accumulated depreciation	-32 161	-31 008
Closing residual value	2 831	2 837
Sum tangible fixed assets	*8 918*	*9 419*

Note 9 *Prepayments and accrued income*

Resources in staff and direct costs spent in ongoing externally funded projects are covered by accrued income until settled by submission of periodic report claims. In 2017 the EGI-engage, EISCAT3D_PfP and VR-OG projects ended and the AARC2 project started.

	2017	2016
Prepaid rents	15	13
Prepaid insurances	207	607
Accrued income, AARC2 project	93	0
Accrued income, COOP_Plus project	63	93
Accrued income, EGI-Engage project	0	348
Accrued income, EISCAT3D_PfP project	0	5 198
Accrued income, ENVRI_Plus project	1 801	561
Accrued income, VR-OG project	0	1 626
Other items	78	84
	2 258	8 530

Note 10 *Bank balances status*

Nordea	76 108	36 317
Cash in hand	1	1
	76 109	36 318

Note 11 *Funds invested status*

Buildings	1 808	2 033
Radar Systems	4 279	4 549
Equipment and Tools	2 831	2 837
	8 918	9 419

Note 12 *Designated funds*

The designated funds are divided into eight funds and reserves. The capital operating and spare parts reserves are used to manage required purchases between years, including unbudgeted ones. The surplus fund is used to manage overall profits and losses between years. The other funds are earmarked for specific purposes.

Two new funds have been created in relation to the started E3DS1 project; E3D construction reserve and decommissioning fund. The first is to handle cost changes in the project and the second is for financing the decommissioning of first the old EISCAT systems being replaced by EISCAT_3D and later, the new systems itself. The new funds will be taken in use 2018 onwards. The net profit for the year will be added to the surplus fund.

Capital operating reserve	1 937	1 942
E3D construction reserve	0	0
Decommissioning fund	0	0
Equipment repair fund	754	754
Investment fund	7 753	7 753
Restructuring reserve	4 101	4 101
Spare parts reserve	119	125
Surplus fund	6 314	5 974
	20 978	20 650

	2017	2016

Note 13 *EISCAT_3D build grants received but not used*

The construction project, E3DS1, started 2017-09-01 and its first phase, Stage 1, will be completed latest 2021-12-31. Four Associates have so far committed to its realisation, the Research Councils in Finland, Norway, Sweden and UK. A funding plan has been agreed and two payments were done in 2017. The funds are kept as prefinancing until used in the project. Funds spent are deducted from the different funding sources in accordance with the agreed funding plan.

RCN (Norway)	0	0
SA (Finland)	0	0
NERC (United Kingdom)	15 450	0
VR (Sweden)	39 985	0
	55 435	0

Note 14 *External project grants received but not used*

All externally funded projects work with prefinancing. For European Commission projects, these are in EUR's. The prefinancing is used to cover reported and approved costs. The MISW and VR-OG projects were financially settled and EGI-Engage and EISCAT3D_PfP projects were both financially concluded during the year. The EISCAT3D_PfP project was financially settled early 2018. The EGI-Engage project remains open due to some reporting issues with other partners in the project consortium. Prefinancing for the new project, AARC2, was received.

AARC2 H2020 prefinancing	300	0
COOP_Plus H2020 prefinancing	1 216	1 181
EGI-Engage H2020 prefinancing	599	479
EISCAT3D_PfP H2020 prefinancing	13 806	13 406
ENVRI_Plus H2020 prefinancing	1 524	1 480
MISW FP7 prefinancing	0	570
VR-OG prefinancing	0	4 000
	17 445	21 115

Stockholm, 2018-05-29

Dr. Tomas Andersson

Dr. Mervyn Freeman

Prof. Hiroshi Miyaoka

Prof. Kenneth Ruud

Dr. Kati Sulonen

Prof. Jian Wu

Dr. Craig Heinselman
Director

Our audit report was issued on 2018-06-14.

Mrs. Annika Wedin
Authorised Public Accountant

pwc

Auditor's report

To the council of EISCAT Scientific Association, corporate identity number 897300-2549

Report on the annual accounts

Opinions

I have audited the annual accounts of EISCAT Scientific Association for the year 2017.

In my opinion, the annual accounts have been prepared in accordance with the Annual Accounts Act and present fairly, in all material respects, the financial position of EISCAT Scientific Association as of 31 December 2017 and its financial performance and cash flow for the year then ended in accordance with the Annual Accounts Act. The statutory administration report is consistent with the other parts of the annual accounts.

Basis for Opinions

I conducted my audit in accordance with International Standards on Auditing (ISA) and generally accepted auditing standards in Sweden. My responsibilities under those standards are further described in the *Auditor's Responsibilities* section. I am independent of EISCAT Scientific Association in accordance with professional ethics for accountants in Sweden and have otherwise fulfilled my ethical responsibilities in accordance with these requirements.

I believe that the audit evidence I have obtained is sufficient and appropriate to provide a basis for my opinions.

Responsibilities of the council and the director

The council and the director are responsible for the preparation of the annual accounts and that they give a fair presentation in accordance with the Annual Accounts Act. The council and the director are also responsible for such internal control as they determine is necessary to enable the preparation of annual accounts that are free from material misstatement, whether due to fraud or error.

In preparing the annual accounts, the council and the director are responsible for the assessment of the association's ability to continue as a going concern. They disclose, as applicable, matters related to going concern and using the going concern basis of accounting. The going concern basis of accounting is however not applied if the council and the director intends to liquidate the association, to cease operations, or has no realistic alternative but to do so.

Auditor's responsibility

My objectives are to obtain reasonable assurance about whether the annual accounts as a whole are free from material misstatement, whether due to fraud or error, and to issue an auditor's report that includes my opinions. Reasonable assurance is a high level of assurance, but is not a guarantee that an audit conducted in accordance with ISAs and generally accepted auditing standards in Sweden will always detect a material misstatement when it exists. Misstatements can arise from fraud or error and are considered material if, individually or in the aggregate, they could reasonably be expected to influence the economic decisions of users taken on the basis of these annual accounts.

As part of an audit in accordance with ISAs, I exercise professional judgment and maintain professional scepticism throughout the audit. I also:

- Identify and assess the risks of material misstatement of the annual accounts, whether due to fraud or error, design and perform audit procedures responsive to those risks, and obtain audit evidence that is

sufficient and appropriate to provide a basis for my opinions. The risk of not detecting a material misstatement resulting from fraud is higher than for one resulting from error, as fraud may involve collusion, forgery, intentional omissions, misrepresentations, or the override of internal control.

- Obtain an understanding of the association's internal control relevant to my audit in order to design audit procedures that are appropriate in the circumstances, but not for the purpose of expressing an opinion on the effectiveness of the association's internal control.
- Evaluate the appropriateness of accounting policies used and the reasonableness of accounting estimates and related disclosures made by the council and the director.
- Conclude on the appropriateness of the councils' and the director's use of the going concern basis of accounting in preparing the annual accounts. I also draw a conclusion, based on the audit evidence obtained, as to whether any material uncertainty exists related to events or conditions that may cast significant doubt on the association's ability to continue as a going concern. If I conclude that a material uncertainty exists, I am required to draw attention in my auditor's report to the related disclosures in the annual accounts or, if such disclosures are inadequate, to modify my opinion about the annual accounts. My conclusions are based on the audit evidence obtained up to the date of my auditor's report. However, future events or conditions may cause the association to cease to continue as a going concern.
- Evaluate the overall presentation, structure and content of the annual accounts, including the disclosures, and whether the annual accounts represent the underlying transactions and events in a manner that achieves fair presentation.

I must inform the council, among other matters, the planned scope and timing of the audit. I must also inform of significant audit findings during my audit, including any significant deficiencies in internal control that I identified.

Report on other legal and regulatory requirements

Opinions

In addition to my audit of the annual accounts, I have also audited the administration of the council and the director of EISCAT Scientific Association for the year 2017. The council and the director have not acted in contravention of the statutes.

Basis for Opinions

I conducted the audit in accordance with generally accepted auditing standards in Sweden. My responsibilities under those standards are further described in the *Auditor's Responsibilities* section. I am independent of EISCAT Scientific Association in accordance with professional ethics for accountants in Sweden and have otherwise fulfilled my ethical responsibilities in accordance with these requirements.

I believe that the audit evidence I have obtained is sufficient and appropriate to provide a basis for my opinions.

Responsibilities of the Council and the director

The council and the director are responsible for the association's organization and the administration of the association's affairs.

Auditor's responsibility

My objective concerning the audit of the administration, and thereby my opinion about discharge from liability, is to obtain audit evidence to assess with a reasonable degree of assurance whether any member of the council or the director in any material respect:

- has undertaken any action or been guilty of any omission which can give rise to liability to the association, or
- in any other way has acted in contravention of the Annual Accounts Act or the statutes.

Reasonable assurance is a high level of assurance, but is not a guarantee that an audit conducted in accordance with generally accepted auditing standards in Sweden will always detect actions or omissions that can give rise to liability to the association.

As part of an audit in accordance with generally accepted auditing standards in Sweden, I exercise professional judgment and maintain professional scepticism throughout the audit. The examination of the administration is based primarily on the audit of the accounts. Additional audit procedures performed are based on my professional judgment with starting point in risk and materiality. This means that I focus the examination on such actions, areas and relationships that are material for the operations and where deviations and violations would have particular importance for the association's situation. I examine and test decisions undertaken, support for decisions, actions taken and other circumstances that are relevant to my opinion.

Gävle, 14 June 2018

Annika Wedin
Authorized Accountant

Appendix:

EISCAT Scientific Association Annual Report, 2018

EISCAT Scientific Association
Registered as a Swedish non-profit organisation
Organisation number: 897300-2549

Annual financial report for the year 2018-01-01 – 2018-12-31

The EISCAT Council and the Director for the Association submits herewith the annual report for 2018.

Content	**Page**
Administration report	2
Profit and loss accounts	5
Balance sheet	6
Statement of cash flows	7
Notes	8

ADMINISTRATION REPORT

Ownership, organisation and objective
The EISCAT Scientific Association was established in 1975 through an agreement between six European organisations. Japan joined in 1996 and the Peoples Republic of China in 2007.

The EISCAT Associates at 2018-12-31 are: China Research Institute of Radiowave Propagation (Peoples Republic of China), National Institute of Polar Research (Japan), Norges forskningsråd (Norway), Suomen Akatemia (Finland), UK Research and Innovation (United Kingdom of Great Britain and Northern Ireland) and Vetenskapsrådet (Sweden).

The now running EISCAT Agreement came into force 2017-06-20, with all Associates making long term funding commitments to the Association. The Association has its formal seat in Kiruna, Sweden, and is registered as a non-profit organisation.

The aim of the Association is to make significant progress in the understanding of physical processes in geospace, in the high latitude atmosphere, and in the coupling between the high and low latitudes and altitudes. For this purpose, the Association has developed, constructed, and now operates, a number of radar facilities at high latitudes. At present, these comprise a system of stations at Tromsö (Norway), Kiruna (Sweden), Sodankylä (Finland), and Longyearbyen (Svalbard). A new system, EISCAT_3D, is currently being constructed.

The Association is fully funded by the Associates, but additional operations may also be funded by short term additional contributions from both Associate and non-Associate bodies. Depending on the available funding, scientific priorities and operational targets are adjusted on an annual basis.

The EISCAT Council is charged with the overall administration and supervision of the Association's activities. The Council appoints a Director, who is responsible for the daily management and operation of the facilities of the Association.

Operation and scientific development
The EISCAT Radars delivered a full programme of operations for the user community and operated reliably throughout the year.

The various EISCAT radars operated for a total of 2 202 accounted hours (2 480 hours in 2017).

Common Programmes amounted to 48% (54%) of the operations. Special Programmes amounted to 45% (41%) and other operations amounted to 7% (5%) of the total hours.

IRAP-CNRS (France), KASI (South Korea), KOPRI (South Korea) and IRA-NASU (Ukraine) have Affiliate agreements and totally 57 hours (10 hours) were affiliates accounted. The Peer-Review Programme made it possible for user groups from P. R. of China, Germany and USA

to run experiments, at no cost, on the systems. Peer-Review time amounted to 99 accounted hours (82 hours).

Future operation and scientific development
All systems are ready for users. These comprise now of the EISCAT Svalbard Radar, Heating and the UHF and VHF radars with the possibility to run the VHF in tristatic mode by using the antennas in Kiruna and Sodankylä for reception.

The EISCAT_3D construction is in full motion. The EISCAT_3D system will replace the current UHF and VHF radar systems. The new system comprises of three phased arrays working together. These will be built in Finland, Norway and Sweden.

The new EISCAT_3D system will be ready for users towards the end of 2021. The old UHF and VHF radar systems will be decommissioned at that time.

Project activities
A new European Commission funded EOSC-Hub "Integrating and managing services for the European Open Science Cloud" project started 2018-01-01.

EISCAT is currently also participating in the AARC2, COOP_Plus and ENVRI_Plus EC-funded projects.

EISCAT_3D project
The now ongoing EISCAT_3D Stage 1 (E3DS1) construction project is well on its way. Three industry contracts were signed during the year and site infrastructure works was planned to start in 2018. Due to geotechnical survey findings at the chosen site in Norway, that work is delayed. The industry contracts relate to deliveries of the antenna system (contractor East China Research Institute of Electronic Engineering – ECRIEE), the receiver system (contractor DA-Design Oy, Finland) and the transmitter system (contractor DA-Design Oy, Finland). Towards the end of 2018, the procurement for the transmitter control system was initiated. The EISCAT_3D construction is fully funded by the EISCAT Associates where Finland, Norway, Sweden and UK have committed substantial amounts. Also P. R. of China and Japan are aiming for funding to EISCAT_3D. The EISCAT_3D project office is co-located with Headquarters and the project team comprises of management, support and engineering expertise. Further staff, particularly IT experts and software developers, will be recruited in 2019.

The work of the Council and its committees
The Council had two ordinary meetings, in May 2018, Stockholm, Sweden and in November 2018 Beijing, P. R. of China. The meetings were chaired by Prof. Hiroshi Miyaoka. At the end of the year, Prof Miyaoka handed over the chairpersonship to Prof. Ingrid Mann. Prof. Mann will be the Council Chairperson for two years, 2019-2020.

The regular Council committees, the Administrative and Finance Committee (AFC) and the Scientific Advisory Committee (SAC) both had two meetings each during the year. The committees meet usually about 1-2 months before the Council meetings.

Budget development during the year

The EISCAT users schedule time on the systems based on research interests and some groups study effects caused by sun activity. Since the solar magnetic activity cycle is currently on minimum level the experiment demand was a bit lower than in other years. This in turn lead to less operations than the nominal target of 2 500 hours.

Less operating hours mean lower costs for operating the systems. Additionally, the radars have functioned well without machinery breakdowns.

In summary, operating costs were below budgeted. The regular grants became higher than budgeted due to favourable exchange rates. The funding agencies commit usually in their own local currencies whereas EISCAT accounts the income in SEK. In total, the year ended in a net profit.

The long-term budget plan

The long-term budget plan is challenging during the transition period where the old systems need to continue operate while EISCAT_3D constructions are done in parallel. In 2021-2022, when EISCAT_3D becomes operational, the old systems being replaced by the new one will be decommissioned. EISCAT_3D will also cost more to operate than the existing systems. Most Associates have though agreed to substantially increase their annual contributions to cover the additional operating costs. The budget plan needs to consider these stages where available staff resources and system availability have to be carefully balanced to manage all requirements.

The result for 2018 and profit/loss handling

The year ended in a net profit of 1 933 kSEK and it is planned to put the amount in the designated funds reserve for use in subsequent years.

PROFIT AND LOSS ACCOUNTS

in thousands of Swedish Crowns

	Note 1	*2018*	*2017*
Income from operations			
Grants received	Note 2	119 127	46 774
Revenue from operations	Note 3	96	89
Other income from operations	Note 4	762	306
		119 984	47 169
Expenses from operations			
Operation costs	Note 5	-6 481	-14 557
Administration costs		-4 102	-4 581
Personnel costs	Note 6	-24 066	-21 884
Depreciation of fixed assets		-5 116	-2 174
		-39 765	-43 197
Operating profit/loss		**80 220**	**3 972**
Financial items			
Interest income		28	12
Other financial income and cost		-1 479	263
		-1 451	275
Net profit/loss for the year		**78 769**	**4 247**

Changes in designated funds	Note 7		
Net profit/loss for the year		78 769	4 247
Use of designated investment funds		-72 047	500
Use of designated funds from previous years		790	11
Allocation of designated funds received during the year, but not used		-5 579	-1 130
Net profit/loss for the year after redistributions		**1 933**	**3 627**

BALANCE SHEET

in thousands of Swedish Crowns

		2018	*2017*
ASSETS			
Fixed assets			
Tangible fixed assets	Note 8		
Buildings		5 059	1 808
Radar systems		87 311	4 279
Equipment and tools		2 261	2 831
		94 631	8 918
Current assets			
Receivables		84 555	24 519
Prepayments and accrued income	Note 9	3 691	2 258
Cash at bank and in hand	Note 10	131 223	76 109
		219 470	102 885
Total assets		**314 101**	**111 804**
CAPITAL AND LIABILITIES			
Capital			
Funds invested	Note 11	94 631	8 918
Designated funds	Note 12	29 395	20 978
Net income for the year after redistribution		1 933	3 627
		125 959	33 524
Current liabilities			
Accounts payable, trade		8 818	5 020
EISCAT_3D build grants received but not used	Note 13	174 823	55 435
External project grants received but not used	Note 14	3 907	17 445
Other liabilities		595	379
		188 142	78 280
Total capital and liabilities		**314 101**	**111 804**

STATEMENT OF CASH FLOWS

in thousands of Swedish Crowns

	2018	*2017*
Operating activities		
Operating result before financial items	80 220	3 972
Transfer from funds invested	5 116	2 174
Interest received	28	12
Currency exchange rate changes	-1 479	263
Extra ordinary income and cost	0	0
Increase/decrease of receivables	-60 037	-22 134
Increase/decrease of prepayments and accrued income	-1 434	6 273
Increase/decrease of creditors and liabilities	109 862	50 905
Cash flow from operations	**132 277**	**41 465**
Investment activities		
Investments in tangible assets	-77 163	-1 674
Cash flow from investment activities	**-77 163**	**-1 674**
Cash flow for the year	**55 114**	**39 791**
Liquid assets at the beginning of the year	**76 109**	**36 318**
Liquid assets at the end of the year	**131 223**	**76 109**

NOTES	2018	2017

Note 1 *Accounting principles*

The accounting and valuation principles applied are consistent with the provisions of the Swedish Annual Accounts Act and generally accepted accounting principles (for 2017 onwards, bokföringsnämnden allmänna råd och vägledningar, BFNAR 2012:1 K3).

All amounts are in thousands of Swedish kronor (SEK) unless otherwise stated.

Income

Received grants are reported as income in the period when they were claimed or received. Conditional grants are recognised as income when the associated conditions have been met. Income and revenue from operations, which include own-account funds, are reported as income when they were claimed or received. Grants and other income in foreign currencies have been accounted in the amounts estimated to be received, based on individual assessment.

Employee benefits

Ongoing remuneration to employees, either direct employed or provided via host agreements, in the form of salaries, social security, contributions to pension schemes and staff related insurances are accounted as personnel costs. Other remunerations, in cash, like travel subsistences or as benefits in-kind, like clothing, training and health care are also accounted as personnel costs. Overhead cost on host provided personnel is considered as external services accounted as administration cost.

Financial income

Dividends and interest income are accounted when credited the account.

Receivables

Receivables are stated at the amounts estimated to be received, based on individual assessment.

Receivables and payables in foreign currencies

Receivables and payables in foreign currencies are valued at the closing day rate. Where hedging measures have been used, such as forwarding contracts, the agreed exchange rate is applied. Gains and losses relating to operations are accounted for under other financial income and cost.

Bank accounts in foreign currencies

Bank balances in foreign currencies are valued at the closing day rate.

Fixed assets

Tangible fixed assets are stated at their original acquisition values after deduction of depreciation according to plan. Assets are depreciated systematically over their estimated useful lives. The following periods of depreciation are applied: Buildings 5 - 50 years, Radar systems 3 - 30 years and Equipment and tools 1 - 5 years.

Note 2 *Grants received*

The Associates contributed to the operation during the year in accordance with the EISCAT agreement. The Affiliates contributed according to agreed annual commitments. Income from European Commission (EC) funded projects were also accounted as received grants. The E3DS1 project started 2017-09-01 and the resulting projects costs were covered by the funding agencies (see also Note 13). All received project grants are first accounted as prefinancing. Project costs are thereafter covered by withdrawals from prefinancing and at that time accounted as income from operations.

	2018	2017
Associates	23 348	22 522
Affiliates	811	796
Project grants, EC	3 078	19 458
Project grant, E3DS1	91 890	1 625
Project grant, VR-OG	0	2 374
	119 127	46 774

Accumulated Associate contributions status as of 2018-12-31

Annual contributions included and for 2018, Japan, Sweden and UK were credited for providing EISCAT_3D and E3DS1 project related funds. These sums are used for EISCAT's ownership and time-share calculation

Associate P. R. of China	41 407	37 245
Associate Finland	89 419	85 559
Associate Japan	95 772	80 057
Associate Norway	183 670	178 203
Associate Sweden	191 915	163 597
Associate UK	310 164	238 187
Previous Associates	382 168	382 168
	1 294 516	1 165 016

Note 3 *Revenue from operations*

The Association can, at rates related to the costs involved and as available, sell observation hours to Associates, Affiliates and other parties. Income from such selling of time are considered to be revenue. In 2018, 8 experiment hours were provided to time-buyers.

Income from time-buyers	96	89

Note 4 *Other income from operations*

The Association supports visiting users by offering site accommodation and equipment hosting for either campaign brought instruments or for longer deployments. Educational support is done by providing teachers and/or other resources (like laboratory support). Associates and/or user-groups contribute occasionally to system improvements by funding, of own interest, certain repairs or hardware changes.

Accommodation	124	143
Instrument hosting agreements	21	21
Educational support	19	18
Other income	597	123
	762	306

Note 5 *Operations*

The annual operating target for all systems together is about 2 500 active (high power mode) hours. For 2018, the budget assumed 2 468 hours and the outcome became 2 072 hours. Passive hours come in addition. Such hours have a minimal effect on cost since the systems do not draw more electricity than in an off mode. Accounted hours are usually lower than the sum of operating hours since some systems have a charge rate that is less than 1-to-1.

Active hours (high-power), per system	*Hours*	*Hours*
EISCAT Svalbard Radar	897	865
UHF system	880	727
VHF system	199	558
Heating system	97	146
	2 072	2 295
Passive hours (receive only)		
Kiruna receiver system	151	444
Sodankylä receiver system	151	444
	302	889

	2018	2017
Accounted hours	*Hours*	*Hours*
Common programmes	1 049	1 356
Special programmes	986	1 012
Other hours	167	113
	2 202	2 480
Distribution of special programme hours between Associates		
Associate P. R. of China	110	107
Associate Finland	156	174
Associate Japan	174	169
Associate Norway	216	278
Associate Sweden	147	193
Associate UK	184	93
	986	1 012
Distribution, other hours		
Affiliates	57	10
EISCAT staff and tests	4	13
Per-reviewed campaigns	99	83
Time-buyers	8	8
	167	113

Note 6 *Personnel costs and average number of employees*

The Association employs directly Headquarters and most project staff, currently about 12 positions, including the Director. Of these, three are on shorter-term project employments. The Headquarters is located in Kiruna, Sweden. The personnel working at the Kiruna (Sweden), Sodankylä (Finland), Svalbard and Tromsø (Norway) sites are normally not employed by the Association. Instead, the personnel are provided via site contracts by the Swedish Institute of Space Physics (Kiruna site staff), Oulu University (Sodankylä staff) and the Arctic University of Norway (Tromsø and Svalbard staff). The Association refunds all expenses related to the provided staff, as well as an additional overhead.

Personnel costs in total		
Salaries and emoluments paid to the Director	1 978	1 920
Other personnel, employed and provided via site contracts	14 598	13 322
Social security contributions amounted to	6 917	6 274
of which for pension costs	*3 248*	*3 061*
Other personnel costs	573	369

The Director, Dr. Craig Heinselman, started his employment 2013-01-01. His current employment contract ends 2021-12-31.

Of the pension costs, 312 kSEK (306 kSEK) relates to the Director. He and all other directly employed staff are included in ITP like occupational pension plans. For the personnel provided via site contracts, the pension plans are handled by their respective employer.

The members of the board (EISCAT Council) and members of committees, who represents Associates and Affiliates, do not receive remunerations from the Association. Travel expenses in connection with Council and committee meetings are normally covered by the Associates and Affiliates. The Association reimburses though the travel costs for Committee Chairpersons and external members.

	2018	2017
Salaries and emoluments and average number of staff per country		
Finland		
Salaries and emoluments	678	453
Average number of staff - men and women	1 + 0	1 + 0
Norway (including Svalbard)		
Salaries and emoluments	5 309	5 314
Average number of staff - men and women	9 + 0	9 + 0
Sweden		
Salaries and emoluments	10 589	9 475
Average number of staff - men and women	12 + 2	10 + 2

Members of the board and Directors at year-end - men and women

The board consist of delegations from every Associate country each having a Delegate (formal member) and up to two Representatives.

Board members (EISCAT Council)	9 + 3	9 + 4
Directors	1 + 0	1 + 0

Note 7 *Changes in designated funds*

Positive numbers - use of designated funds. Negative - transfer to the reserve or fund for later use.

Net profit/loss for the year	78 769	4 247
Changes to capital operating reserve	182	4
Changes to decommissioning fund	-2 446	0
Changes to E3D construction reserve	-3 134	0
Changes to funds invested	-72 047	500
Changes to spare parts reserve	18	6
Changes to surplus fund	590	-1 130
	1 933	3 627

Note 8 *Tangible fixed assets*

Changes in tangible fixed assets.

Buildings		
Opening acquisition value	42 478	42 471
Acquisitions during the year	3 544	6
Disposals during the year	0	0
Closing acquisition value	46 021	42 478
Opening accumulated depreciation	-40 670	-40 439
Depreciations during the year	-293	-231
Disposals during the year	0	0
Closing accumulated depreciation	-40 963	-40 670
Closing residual value	5 059	1 808
Radar systems		
Opening acquisition value	250 760	250 259
Acquisitions during the year *	86 597	501
Disposals during the year	0	0
Closing acquisition value	337 357	250 760
Opening accumulated depreciation	-246 480	-245 709
Depreciations during the year	-3 566	-771
Disposals during the year	0	0
Closing accumulated depreciation	-250 047	-246 480
Closing residual value	87 311	4 279

* Whereof 13 665 kSEK relates to in-kind provided parts from NIPR, Japan

	2018	2017
Equipment and tools		
Opening acquisition value	34 992	33 844
Acquisitions during the year	687	1 166
Disposals during the year	27	19
Closing acquisition value	35 652	34 992
Opening accumulated depreciation	-32 161	-31 008
Depreciations during the year	-1 257	-1 172
Disposals during the year	27	19
Closing accumulated depreciation	-33 391	-32 161
Closing residual value	2 261	2 831
Sum tangible fixed assets	94 631	8 918

Note 9 *Prepayments and accrued income*

Resources in staff and direct costs spent in ongoing externally funded projects are covered by accrued income until settled by submission of periodic report claims. In 2018 the EOSC-hub project started.

Prepaid rents	1	15
Prepaid insurances	698	207
Accrued income, AARC2 project	120	93
Accrued income, COOP_Plus project	895	63
Accrued income, ENVRI_Plus project	1 149	1 801
Accrued income, EOSC-hub project	710	0
Other items	118	78
	3 691	2 258

Note 10 *Bank balances status*

Nordea	131 223	76 108
Cash in hand	0	1
	131 223	76 109

Note 11 *Funds invested status*

Buildings	5 059	1 808
Radar Systems	87 311	4 279
Equipment and Tools	2 261	2 831
	94 631	8 918

Note 12 *Designated funds*

The designated funds are divided into eight funds and reserves. The capital operating and spare parts reserves are used to manage required purchases between years, including unbudgeted ones. The surplus fund is used to manage overall profits and losses between years. The other funds are earmarked for specific purposes.

Capital operating reserve	1 755	1 937
E3D construction reserve	3 134	0
Decommissioning fund	2 446	0
Equipment repair fund	754	754
Investment fund	7 753	7 753
Restructuring reserve	4 101	4 101
Spare parts reserve	101	119
Surplus fund	9 351	6 314
	29 395	20 978

	2018	2017

Note 13 *EISCAT_3D build grants received but not used*

The construction project, E3DS1, started 2017-09-01 and its first phase, Stage 1, will be completed latest 2021-12-31. Four Associates have so far committed to its realisation, the Research Councils in Finland, Norway, Sweden and UK. A funding plan has been agreed and seven payments were done in 2018. The funds are kept as prefinancing until used in the project. Funds spent are deducted from the different funding sources in accordance with the agreed funding plan.

Changes in EISCAT_3D build grants received but not used

Associate Finland		
Opening balance	0	0
Received during the year	41 109	0
Used during the year	0	0
Closing balance	41 109	0
Associate Norway		
Opening balance	0	0
Received during the year	66 381	0
Used during the year	0	0
Closing balance	66 381	0
Associate Sweden		
Opening balance	39 980	0
Received during the year	50 000	40 000
Used during the year	-22 648	-20
Closing balance	67 332	39 980
Associate UK		
Opening balance	15 455	0
Received during the year	53 787	17 060
Used during the year	-69 242	-1 605
Closing balance	0	15 455
Sum EISCAT_3D received build grants	174 823	55 435

Note 14 *External project grants received but not used*

All externally funded projects work with prefinancing. For European Commission projects, these are in EUR's. The prefinancing is used to cover reported and approved costs. The EGI-Engage and EISCAT3D_PfP projects were both concluded during 2017 and financially settled in 2018. Prefinancing for the new project, EOSC-hub, was received.

AARC2 H2020 prefinancing	57	300
COOP_Plus H2020 prefinancing	1 110	1 216
EGI-Engage H2020 prefinancing	0	599
EISCAT3D_PfP H2020 prefinancing	0	13 806
ENVRI_Plus H2020 prefinancing	1 509	1 524
EOSC-hub prefinancing	1 230	0
	3 907	17 445

Tokyo 2019-06-11

Dr. Tomas Andersson

Dr. Mervyn Freeman

Prof. Hiroshi Miyaoka

Prof. Kenneth Ruud

Dr. Kati Sulonen

Prof. Jian Wu

Dr. Craig Heinselman
Director

Our audit report was issued on 2019-06-24
Öhrlings PricewaterhouseCoopers AB

Mrs. Annika Wedin
Authorised Public Accountant

Auditor's report

To the council of EISCAT Scientific Association, corporate identity number 897300-2549

Report on the annual accounts

Opinions

I have audited the annual accounts of EISCAT Scientific Association for the year 2018.

In my opinion, the annual accounts have been prepared in accordance with the Annual Accounts Act and present fairly, in all material respects, the financial position of EISCAT Scientific Association as of 31 December 2018 and its financial performance and cash flow for the year then ended in accordance with the Annual Accounts Act. The statutory administration report is consistent with the other parts of the annual accounts.

Basis for Opinions

I conducted my audit in accordance with International Standards on Auditing (ISA) and generally accepted auditing standards in Sweden. My responsibilities under those standards are further described in the *Auditor's Responsibilities* section. I am independent of EISCAT Scientific Association in accordance with professional ethics for accountants in Sweden and have otherwise fulfilled my ethical responsibilities in accordance with these requirements.

I believe that the audit evidence I have obtained is sufficient and appropriate to provide a basis for my opinions.

Responsibilities of the council and the director

The council and the director are responsible for the preparation of the annual accounts and that they give a fair presentation in accordance with the Annual Accounts Act. The council and the director are also responsible for such internal control as they determine is necessary to enable the preparation of annual accounts that are free from material misstatement, whether due to fraud or error.

In preparing the annual accounts, the council and the director are responsible for the assessment of the association's ability to continue as a going concern. They disclose, as applicable, matters related to going concern and using the going concern basis of accounting. The going concern basis of accounting is however not applied if the council and the director intends to liquidate the association, to cease operations, or has no realistic alternative but to do so.

Auditor's responsibility

My objectives are to obtain reasonable assurance about whether the annual accounts as a whole are free from material misstatement, whether due to fraud or error, and to issue an auditor's report that includes my opinions. Reasonable assurance is a high level of assurance, but is not a guarantee that an audit conducted in accordance with ISAs and generally accepted auditing standards in Sweden will always detect a material misstatement when it exists. Misstatements can arise from fraud or error and are considered material if, individually or in the aggregate, they could reasonably be expected to influence the economic decisions of users taken on the basis of these annual accounts.

As part of an audit in accordance with ISAs, I exercise professional judgment and maintain professional scepticism throughout the audit. I also:

- Identify and assess the risks of material misstatement of the annual accounts, whether due to fraud or error, design and perform audit procedures responsive to those risks, and obtain audit evidence that is

sufficient and appropriate to provide a basis for my opinions. The risk of not detecting a material misstatement resulting from fraud is higher than for one resulting from error, as fraud may involve collusion, forgery, intentional omissions, misrepresentations, or the override of internal control.

- Obtain an understanding of the association's internal control relevant to my audit in order to design audit procedures that are appropriate in the circumstances, but not for the purpose of expressing an opinion on the effectiveness of the association's internal control.
- Evaluate the appropriateness of accounting policies used and the reasonableness of accounting estimates and related disclosures made by the council and the director.
- Conclude on the appropriateness of the councils' and the director's use of the going concern basis of accounting in preparing the annual accounts. I also draw a conclusion, based on the audit evidence obtained, as to whether any material uncertainty exists related to events or conditions that may cast significant doubt on the association's ability to continue as a going concern. If I conclude that a material uncertainty exists, I am required to draw attention in my auditor's report to the related disclosures in the annual accounts or, if such disclosures are inadequate, to modify my opinion about the annual accounts. My conclusions are based on the audit evidence obtained up to the date of my auditor's report. However, future events or conditions may cause the association to cease to continue as a going concern.
- Evaluate the overall presentation, structure and content of the annual accounts, including the disclosures, and whether the annual accounts represent the underlying transactions and events in a manner that achieves fair presentation.

I must inform the council, among other matters, the planned scope and timing of the audit. I must also inform of significant audit findings during my audit, including any significant deficiencies in internal control that I identified.

Report on other legal and regulatory requirements

Opinions

In addition to my audit of the annual accounts, I have also audited the administration of the council and the director of EISCAT Scientific Association for the year 2018. The council and the director have not acted in contravention of the statutes.

Basis for Opinions

I conducted the audit in accordance with generally accepted auditing standards in Sweden. My responsibilities under those standards are further described in the *Auditor's Responsibilities* section. I am independent of EISCAT Scientific Association in accordance with professional ethics for accountants in Sweden and have otherwise fulfilled my ethical responsibilities in accordance with these requirements.

I believe that the audit evidence I have obtained is sufficient and appropriate to provide a basis for my opinions.

Responsibilities of the Council and the director

The council and the director are responsible for the association's organization and the administration of the association's affairs.

Auditor's responsibility

My objective concerning the audit of the administration, and thereby my opinion about discharge from liability, is to obtain audit evidence to assess with a reasonable degree of assurance whether any member of the council or the director in any material respect:

- has undertaken any action or been guilty of any omission which can give rise to liability to the association, or
- in any other way has acted in contravention of the Annual Accounts Act or the statutes.

Reasonable assurance is a high level of assurance, but is not a guarantee that an audit conducted in accordance with generally accepted auditing standards in Sweden will always detect actions or omissions that can give rise to liability to the association.

As part of an audit in accordance with generally accepted auditing standards in Sweden, I exercise professional judgment and maintain professional scepticism throughout the audit. The examination of the administration is based primarily on the audit of the accounts. Additional audit procedures performed are based on my professional judgment with starting point in risk and materiality. This means that I focus the examination on such actions, areas and relationships that are material for the operations and where deviations and violations would have particular importance for the association's situation. I examine and test decisions undertaken, support for decisions, actions taken and other circumstances that are relevant to my opinion.

Gävle, 24 June 2019

Annika Wedin
Authorized Accountant

Report 2017–2018 of the EISCAT Scientific Association

©EISCAT Scientific Association
EISCAT Headquarters
Box 812, SE-981 28 Kiruna, Sweden

Scientific contributions: EISCAT Associates and staff

The EISCAT Associates and Affiliates

December 2018

CRIRP

China Research Institute of Radiowave Propagation
China
www.crirp.ac.cn

NFR

Forskningsrådet
Norway
www.forskningsradet.no

NIPR

National Institute of Polar Research
Japan
www.nipr.ac.jp

SA

Suomen Akatemia
Finland
www.aka.fi

UKRI

UK Research and Innovation
United Kingdom
www.ukri.org

VR

Vetenskapsrådet
Sweden
www.vr.se

IRAP

Institut de Recherche en Astrophysique et Planétologie
France
www.irap.omp.eu

KASI

Korea Astronomy and Space Science Institute
South Korea
www.kasi.re.kr

KOPRI

Korea Polar Research Institute
South Korea
www.kopri.re.kr

RIAN

Institute of Radio Astronomy
Ukraine
rian.kharkov.ua

EISCAT Scientific Association

Headquarters

EISCAT Scientific Association
Box 812
SE-981 28 Kiruna, Sweden
Phone: +46 980 79150
www.eiscat.se

Sites

Kiruna

EISCAT Kiruna Site
Box 812
SE-981 28 Kiruna, Sweden
Phone: +46 980 79150

Longyearbyen

EISCAT Svalbard Radar
Postboks 432
N-9171 Longyearbyen, Svalbard
Phone: +47 776 25270

Sodankylä

EISCAT Sodankylä Site
Tähteläntie 54B
FIN-99600 Sodankylä, Finland

Tromsø

EISCAT Tromsø Site
Ramfjordmoen
N-9027 Ramfjordbotn, Norway
Phone: +47 776 20730